論文 / 著書情報
Article / Book Information

題目(和文)	微小圧縮試験を用いた電析金属の機械的特性評価
Title(English)	Mechanical Property Evaluation of Electrodeposited Metals by Using Micro-Compression Test
著者(和文)	名越貴志
Author(English)	Takashi Nagoshi
出典(和文)	学位:博士(工学), 学位授与機関:東京工業大学, 報告番号:甲第9504号, 授与年月日:2014年3月26日, 学位の種別:課程博士, 審査員:曽根　正人,里　達雄,加藤　雅治,細田　秀樹,稲邑　朋也
Citation(English)	Degree:Doctor (Engineering), Conferring organization: Tokyo Institute of Technology, Report number:甲第9504号, Conferred date:2014/3/26, Degree Type:Course doctor, Examiner:,,,,
学位種別(和文)	博士論文
Type(English)	Doctoral Thesis

Mechanical Property Evaluation of Electrodeposited Metals by Using Micro-Compression Test

Doctor of Engineering

Department of Materials Science and Engineering

Tokyo Institute of Technology

Takashi Nagoshi

2014

Contents

CHAPTER 1

General introduction

1.1 Micro-testing

Micro-sized testing, whose sample size is in a micron regime, has great interests in many fields. According to Japanese Industrial Standards, material mechanical property evaluation requires gage length larger than the 10 mm for tensile, bend, compression testing. On the other hands, micro-sized testing which using micron-sized specimen can evaluate local mechanical properties such as thermally affected area with thermal gradient like welding and abrasion damaged surface area. More importantly, these micro-tests can be conducted with keep equipment almost intact and therefore useful for lifetime expectations of working plants.

Besides testing methods for structural materials, micro-sized components itself has been used in micro-electro-mechanical systems (MEMS). Recent developments of MEMS are outstandingly fast and needs improved performance,

reliable devise lifetime, and smaller devise size. MEMS are made up of components below 100 μm in size. For example, MEMS based accelerometers or gyroscopes were widely used in cell phones, gaming consoles and location-based devices. Some more examples shown in figure 1-1 are optical switch (1-1a), gyro sensor (1-1b), and micro-windmill (1-1c) [1]. Micro-components used in MEMS such as micro-spring, bending beams, and structural support of MEMS suffer from mechanical straining and needs suitable mechanical properties. However, at these size scales, the classical physics are not always useful. Sample size effect, which described in latter section, emerges. Thus, the micro-testing method with specimen whose sample size is in same scales with actual MEMS components is needed.

1.2 Mechanical properties of small scale materials

Intrinsic length scale represented by its microstructures such as grain boundaries and dislocation arrangements has been all time concern in material science. In recent decades, extrinsic length scale i.e. sample size has known to have influence on mechanical properties at a several tens of micron and smaller. In particular, the strength of metals has been shown to increase with decreasing sample

size, known as “smaller is stronger” also referred to as size effect [2]. For example, thin film experiments, including wafer curvature [3,4] micro tensile tests [5,6], bulge tests [7,8] and MEMS based tests [9], have consistently shown an increase of strength with decreasing sample size. Size effect in bending [10], torsion [11], or indentation [12,13] has been explained by plastic strain gradient. Assuming geometrically necessary dislocation responsible for plastic deformation, larger densities of dislocations in small scale materials has large flow stress [11,14,15]. However, even in the absence of strain gradients for compression pillar, they exhibit size dependent yield stress for different single crystalline metals such as nickel [16,17], gold [18,19], copper [20] and aluminum [21]. Frick et al. reported that the [111] nickel pillars with diameters of about 200 nm has strength of more than 2 GPa which significantly higher than bulk counterparts but lower than the theoretical strength [19]. Furthermore, for face-centered cubic (fcc) metals and alloys, shear flow stress normalized by shear modulus and pillar diameter normalized by magnitude of burgers vector has power low relationships with exponent of -0.66 [22] as shown in figure 1-2. Greer et al. proposed dislocation starvation theory for explanation of size dependent strength of compression pillars [20,23,24]. The model assumes that the small sample will starve of mobile dislocations if the rate of

dislocation ejection at the free surface is larger than the rate of dislocation multiplication via double cross-slip or similar processes. In dislocation starved samples, new dislocations have to be nucleated from dislocation sources. The size effect is then rationalized by the correlation of source size with sample size leading to higher yield stresses for smaller pillars. This model is supported by simulations [25,26] and post transmission electron microscopy (TEM) observation [21.27], as well as in situ TEM experiments [28].The majority of research investigating the size effect of metals by means of the micro-testing technique has focused on single crystalline metals and alloys. Only limited data exists for metals with microstructures. The studies by Rinaldi et al. [29] and Jang and Greer [30] have investigated nickel nanocrystalline nano-pillars. However, their trends for strength as a function of sample size showed opposite trend: Jang and Greer observe a “smaller is weaker” power-law dependence with the exponent of 0.15 while Rinaldi et al. show very scattered result for 30 nm-grained nanocrystalline nickel which exhibit the slight strengthening with decreasing sample size. Moreover, their nano-pillar has very similar scale parameter for extrinsic sample size d and intrinsic grain size D, compression pillar by Rinaldi et al. has 5 and 10 of d/D and by Jang and Greer has ranged 30 to 2 of d/D. Size effect proposed by Armstrong [31] which arises when

few grains are present in a specimen, and this effect is due mainly to the orientation dependence of crystal plastic flow. Thus, currently the experimental findings for sample size effect on nanocrystalline materials are inconclusive and there is much uncertainty with respect to the deformation mechanism and combined effect of different size effects. Sample size effect on polycrystalline pillar has great interest in industries owing to miniaturization of MEMS devices reaching to its component scales at sub-micron or nano regime.

1.3 Electrodeposition with supercritical CO_2 emulsion

MEMS devises usually fabricated using film formation process. Process for metallic film formation has two large classifications, one is dry process and the other is wet process. Former process use gas or metallic vapor for deposition or directly deposit metal atoms at the surface by sputtering. Process is simple, but the deposition rate is very slow like sub-nm to several nm in a second [32,33]. Thus the deposition is limited to sub-μm in industrial applications and not favorable for fabrication of MEMS components which require structural support. One of the wet process, electroplating have been used in industrial for fabrication of MEMS and integrated

circuit (IC) thanks to the fast deposition rate, low cost production, and simple operation [34,35]. In recent years, miniaturization of MEMS and IC merges into nano-scale regime, so-called nanotechnology. Component size or wire width reaches several tens of nanometers. For fabrication, gaps with an inversed geometry filled with metals by deposition process. In the filling of small gaps, some problems arise as schematically shown in figure 1-3. Since liquid solutions were used in wet process, if the substrate not covered with electrolyte or hydrogen gas bubbles evolved in the reaction on the substrate, these area left unfilled and voids and pin-holes formed [36].

To accomplish successful metal gap-fill, we have developed electroplating method with supercritical CO_2 emulsion (ESCE) [37,38]. In this system, micelles formed with surfactant which encapsulates supercritical CO_2. These micelles randomly bounce on the surface of cathode and desorb hydrogen bubbles evolved. Bouncing micelles will give an uniform distributions of metal ions at the surface. These features will contribute to the gap or hole filling in ESCE, and attained filling of hole with 70 nm in diameter and 350 nm in depth as shown in figure 1-4 [39].

1.4 Motivations and aims of this study

We have been developed electroplating technique with supercritical CO_2 emulsion. However, mechanical testing method suitable for micro-sized metals has not been established. In addition, sample size effect on the polycrystalline metals is not clarified yet. Therefore, we developed micro-testing method with micro-sized specimen to study mechanical properties of electrodeposited metallic materials.

Chapter 2 confirms an availability of micro compression testing which allows evaluation of strength and uniform strain of fine structured materials. The effect of strain amount by severe plastic deformation (SPD) on microstructure, grain boundary characteristics, and mechanical properties was quantified and discussed.

In Chapter 3, Mechanical properties of copper deposited by ESCE were evaluated. Observed microstructure change in room temperature storage was investigated and compared with copper electroplated by conventional method.

Chapter 4 discusses high mechanical properties of nickel film fabricated by ESCE. Mechanical properties were evaluated by proposed micro-compression test using non-tapered square pillar. Effect of microstructure on mechanical properties was investigated based on Hall-Petch (H-P) relationship.

Chapter 5 investigates sample size effect on mechanical properties of nanocrystalline nickel fabricated by ESCE with comparison to single crystal counterparts. Observed sample size effect was discussed based on the deformation behavior of nanocrystalline materials.

1.5 References

[1] E. Giomi, L. Fanucci, A. Rocchi Microelectron. J., 2013 In Press

[2] E. Arzt, Acta Mater., 46 (1998) 5611.

[3] G. Dehm, T. Wagner, T.J. Balk, E. Arzt, B.J. Inkson, J. Mater. Sci. Tech., 18 (2002) 113.

[4] G. Dehm, T.J. Balk, H. Edongue, E. Arzt, Microelectron. Eng., 70 (2003) 412.

[5] P.A. Gruber, J. Bohm, F. Onuseit, A. Wanner, R. Spolenak, E. Arzt, Acta Mater., 56 (2008) 2318.

[6] P.A. Gruber, C. Solenthaler, E. Arzt, R. Spolenak, Acta Mater., 56 (2008) 1876.

[7] Y. Xiang, X. Chen, J.J. Vlassak, J. Mater. Res., 20 (2005) 2360.

[8] Y. Xiang, T.Y. Tsui, J.J. Vlassak, J. Mater. Res., 21 (2006) 1607.

[9] M.A. Haque, M.T.A. Saif, Experimental Mech., 43 (2003) 248.

[10] J.S. Stölken, A.G. Evans,Acta Mater., 46 (1998) 5109.

[11] N.A. Fleck, G.M. Muller, M.F. Ashby, J.W. Hutchinson, Acta Metall. Mater., 42 (1994) 475.

[12] W.D. Nix, Metall. Trans. A, 20 (1989) 2217.

[13] Q. Ma, D.R. Clarke, J.Mater. Res., 10 (1995) 853.

[14] H. Gao, Y. Huang, W.D. Nix, J.W. Hutchinson, J.Mech. Phys. Solids, 47 (1999) 1239.

[15] Y. Huang, H. Gao, W.D. Nix, J.W. Hutchinson, J. Mech. Phys. Solids, 48 (2000) 99.

[16] D.M. Dimiduk, M.D. Uchic, T.A. Parthasarathy, Acta Mater., 53 (2005) 4065.

[17] C.P. Frick, B.G. Clark,S. Orso, A.S. Schneider, E. Arzt, Mater. Sci. Eng. A, 489 (2008) 319.

[18] J.R. Greer, W.C. Oliver, W.D.Nix, Acta Mater., 53 (2005) 1821.

[19] C.A. Volkert, E.T. Lilleodden, Philos. Mag., 86 (2006) 5567.

[20] D. Kiener, C. Motz, G. Dehm, Mater. Sci. Eng. A, 505 (2009) 79.

[21] K.S. Ng, A.H.W. Ngan, Acta Mater., 56 (2008) 1712.

[22] J.R. Greer, J.T.M De Hosson, Prog. Mater. Sci., 56 (2011) 654.

[23] S.S. Brenner, J. Appl. Phys., 28 (1957) 1023.

[24] J.R. Greer, Rev. Adv. Mater. Sci., 13 (2006) 59.

[25] V.S. Deshpande, A. Needleman, E. Van der Giessen, J. Mech. Phys. Solids, 53(2005) 2661.

[26] D.S. Balint, V.S. Deshpande, A. Needleman, E. Van der Giessen, Modelling Simul. Mater. Sci. Eng., 14 (2006) 409.

[27] A.A. Benzerga, N.F. Shaver, Scripta Mater., 54 (2006) 1937.

[28] Z.W. Shan, R.K. Mishra, S.A.S. Asif, O.L. Warren, A.M. Minor, Nature Mater., 7 (2008) 115.

[29] A. Rinaldi, P. Peralta, C. Friesen, K. Sieradzki, Acta. Mater., 56 (2008) 2652.

[30] D. Jang, J.R. Greer, Scripta Mater., 64 (2011) 77.

[31] R.W. Armstrong, J. Mech. Phys. Solids, 9 (1961) 196.

[32] Y. Sun, T. Miyasato, J.K. Wigmore N. Sonoda, Y. Watari, J. Appl. Phys., 82 (1997) 2334.

[33] T. Yoshida, T Tani, H Nishimura, K, Akashi J. Appl. Phys., 54 (1983).

[34] M. Gad-el-Hak, *The MEMS Handbook*; CRC, Taylor & Francis: Boca Raton, Fla., 2006.

[35] J.W. Schultze, A. Bressel, Electrochimica Acta, 47 (2001) 3.

[36] W.L. Tsai, P.C. Hsu, Y. Hwu, C.H. Chen, L.W. Chang, J.H. Je, M.H. Lin, A. Groso, G. Margaritondo, Nature, 417 (2002) 139.

[37] H. Yoshida, M. Sone, H. Wakabayashi, H. Yan, K. Abe, X.T. Tao, A. Mizushima, S. Ichihara, S. Miyata, Thin Solid Films, 446 (2004) 194.

[38] H. Yan, M. Sone, N. Sato, S. Ichihara, S. Miyata, Surf. Coat. Tech., 182 (2004) 329.

[39] N. Shinoda, T. Shimizu, T.F.M. Chang, A. Shibata, M. Sone, microelectron. Eng., 97C (2012) 126.

1.6 Figures

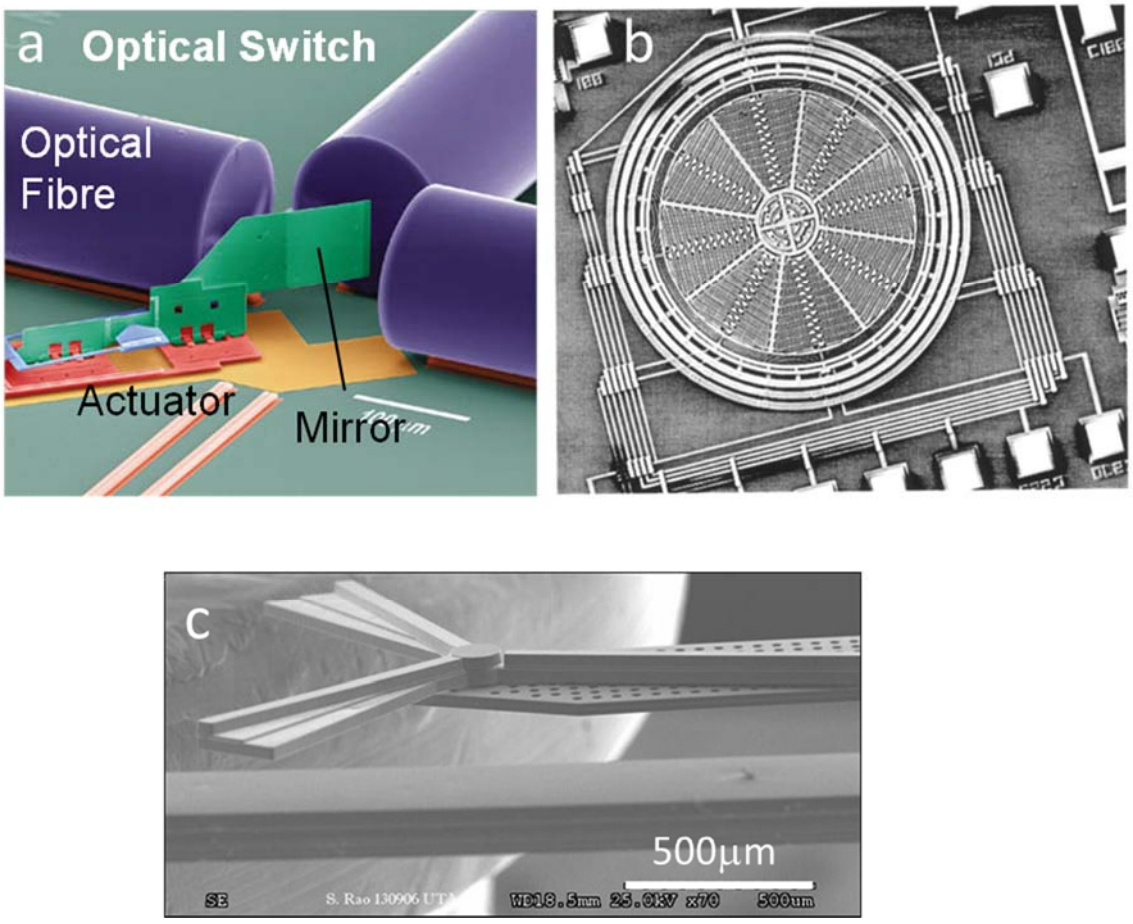

Figure 1-1 Examples of MEMS devises (a) optical switch, (b) gyro sensor (c) micro-windmill

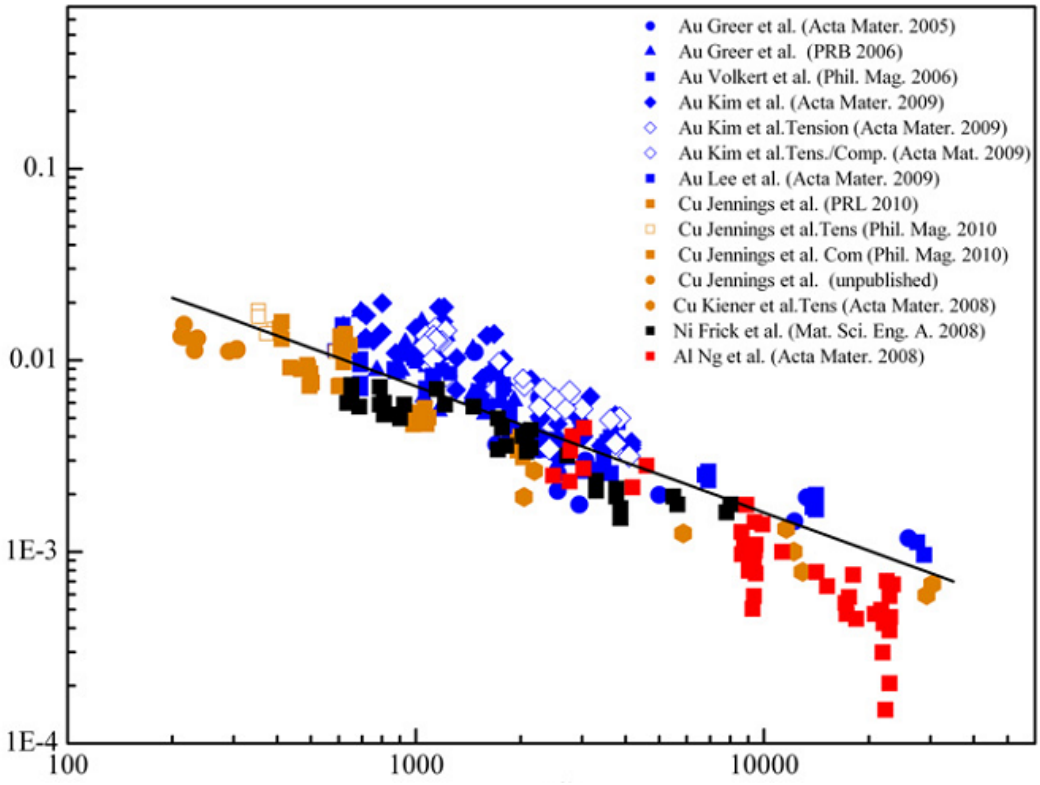

Figure 1-2. Shear flow stress normalized by shear modulus on appropriate slip system for most face-centered cubic metallic micro- and nano-pillars tested in compression and tension to date [22].

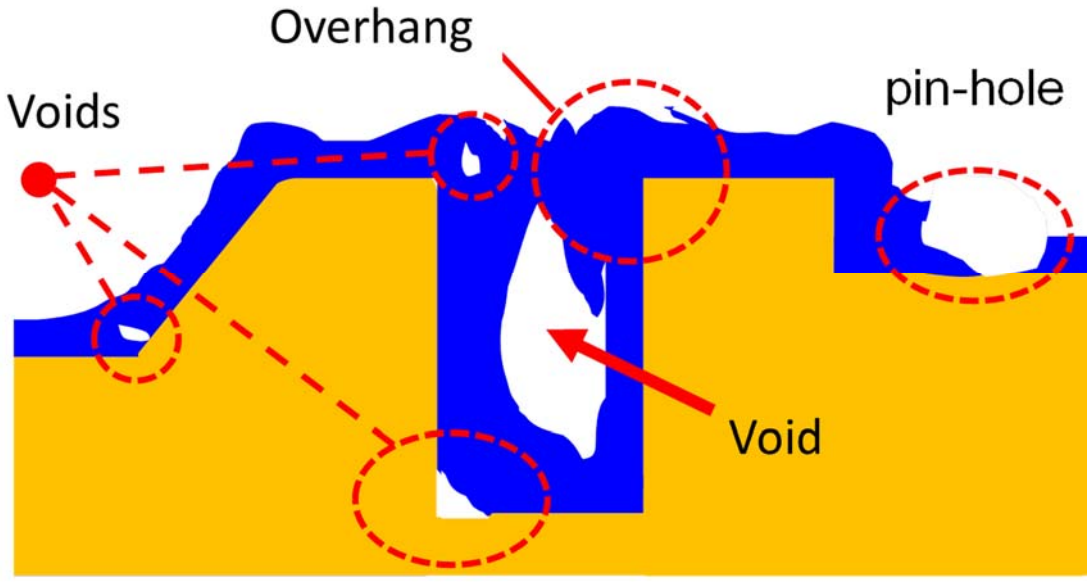

Figure 1-3. Failures found in filling of gaps with electrodeposition.

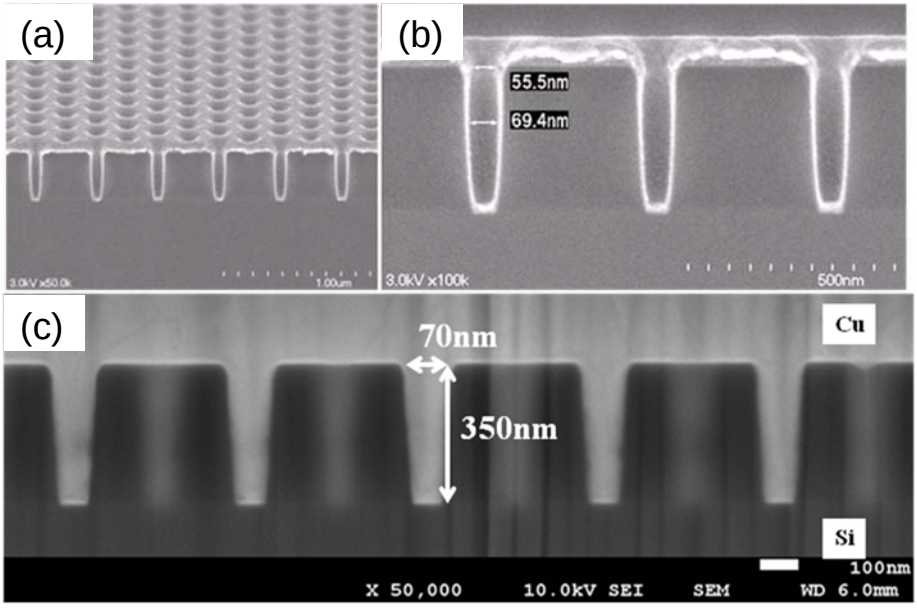

Figure 1-4. Cross sectional SEM images of (a) Hole test element group (TEG) with holes of 70 nm in diameter and aspect ratio of 5, (b) expanded image of (a), and (c) TEG filled with Cu electroplated in ESCE with copper particles.

CHAPTER 2

Mechanical properties of high pressure torsion processed ferrite

2.1 Introduction

In recent years, fabrication of ultrafine grained (UFG) metals and alloys using SPD process such as high pressure torsion (HPT) [1,2], equal-channel angular pressing (ECAP) [1,3], and accumulative roll bonding (ARB) [4] have been attractive research topics. The unusual and extraordinary mechanical properties of the UFG materials have attracted considerable interests among many researchers. These features are related to the grain boundaries owing to larger volume fraction of grain boundary area and interaction with mobile dislocation in small grains for UFG materials. UFG materials fabricated by SPD process have grain boundaries containing extensive number of defects such as dislocations and vacancies which termed as non-equilibrium grain boundary [1,5,6,7]. Characteristics of the grain boundary (e.g. equilibrium, non-equilibrium, coincidence site lattice, misorientation angle) play an important role in deformation behavior [1,8,9].

In tensile tests of the UFG materials, yield drop phenomenon, Luder's band formation, and shear banding are observed [10] unlike in their conventional grain size counterparts. Elongation decreases abruptly as the grain size decreases to 1 μm. In this grain size regime, necking can occur accompanied by localized shear. Outside of the necked section, surface observation does not show any sign of deformation. This sudden drop of elongation is also observed in UFG interstitial-free steel and aluminum [11]. The lack of dislocation storage due to decreasing grain size is responsible to the notable decrease in work hardening capability. When the grain size becomes smaller than 1 μm, work hardening does not work to maintain the shape of deformed area resulting in early failure. Because of this early failure, observation of work hardening behavior is not available in tensile test. Therefore, compression testing is needed to investigate the deformation behavior in wide range of strain amount. Observation of the deformation behavior in UFG materials with wide range of strain is a main subject of this section

In this work, we used HPT to refine the grains of ultra-low carbon steel. HPT process introduces large amount of torsional strain to the periphery of the disk shaped materials. Materials subjected to such non-homogeneous deformation with

large strain and large strain gradient have different crystallographic or structural features within the specimen [12]. Bulk sized testing, which is widely used as a mechanical testing method, normalizes effects of such difference on mechanical properties. On the contrary, site specific response of mechanical properties can be obtained using micro-sized test specimen fabricated by FIB from the area of interest. As widely accepted, strengths of materials are increased with decreasing dimensions of micro or sub-micro scale. Uchic et al. reported that micro-compression with 10 μm in diameter samples displayed a mechanical response that matched the behavior of bulk tension test [13]. Present micro-compression test was with 20 μm of pillars, which is expected to show representative comparable mechanical properties with bulk counterparts. Micro-pillars fabricated from HPT processed disk were evaluated by compression test to investigate site specific mechanical properties with the microstructures observed by EBSD analysis.

2.2 Experimental procedures

Starting material of this work was ultra-low carbon steel (11C, <30Si, 20P, <3S <2B 8N, 14O, 300Al, <20Ti, <30Cr, <30Cu, in mass ppm). Homogenization

treatment was conducted at 1273 K for an hour in pure Ar atmosphere. After homogenization, material was cut and polished into disks of 10 mm in diameter and 0.85 mm in thickness to subject to the HPT process. Using two anvils holding disk, materials were subjected to torsional strain for one or five rotations at a rotation speed of 0.2 rpm under a hydrostatic pressure of 5 GPa. Recorded processing temperature of the anvil increased only several degrees during HPT process. Details of HPT process has been described elsewhere [14,15].

For fabrication of the micro-sized compression pillar and investigation of the microstructures, HPT processed disks were cut and polished mechanically followed by electrolytic polishing using a solution of 900 ml CH_3COOH + 100 ml $HClO_4$. This etching process removed deformation layer by cutting and mechanical polishing and improved qualities in further orientation mapping. The samples were mounted on holders to ease further handling and to ensure alignment for uniaxial compression test.

The microstructures and grain boundary characteristics were examined by SEM (S-4500SE: Hitachi) equipped with EBSD (INCA Crystal software: Oxford instruments) from the electrolytic polished surface which normal to the torsional axis.

The scanning step size corresponding to the size of pixels in orientation map was 30 nm. Compression pillars were fabricated by FIB from the region analyzed by EBSD technique. Sequences of pillar fabrication are illustrated in figure 2-1 with corresponding scanning ion microscope (SIM) images. In the course of fabrication, we first made a pillar which has the thickness of thin plate which is around 100 μm as shown in figure 2-1 (a). Using irradiation of 45 degrees from thin plate, we made a small pillar from the bigger one as shown in figure 2-1 (b). Ion beam from side of the specimen allowed the fabrication of a pillar with uniform dimensions (non-tapered, non-filleted). Finally, we milled each side of the pillar at a tilt angle of ±2.3 degrees with 400 pA ion beam to minimize ion bombardment damage. The pillar had 20 μm on a side with square cross-section and 30 μm in height. The sample had an aspect ratio of 1:1.5.

Compression tests were carried out in room temperature using a test machine specifically designed for micro-sized specimens assembled in our laboratory. The details of which are described in previous paper [16]. This testing machine enables us to demonstrate single stroke compression up to 32 μm of displacement, while other nanoindentation module utilized micro-compression test usually needs

multiple cycles of loading/unloading. A flat ended diamond tip with 50 μm diameter equipped to piezoelectric loading device applies displacement to the specimen. During compression, displacement of the tip was controlled at a constant rate of 0.1 μm/s which result in strain rate of 0.003 s^{-1}. The data of displacement and load were recorded at a rate of 30 data points per second.

2.3 Results and discussion

2.3.1 EBSD analysis

Crystal orientations of the materials were determined using SEM/EBSD. Figure 2-2 shows the orientation map of UFG ferrite obtained by EBSD analysis. The grains are slightly elongated to shear direction in upper side of the images indicated by the black arrow. Grain size is defined as the diameter of an equivalent circle having the same area surrounded by grain boundary with misorientation larger than 15 degrees in orientation maps. The grain sizes of each area with different strain amount are shown in Table 2-1. Grain size was reduced to 300 nm in the sample deformed with 1 rotation (N=1) at 3 mm away from center which had a shear strain amount of 31 (γ=31). Further increase in the number of rotation or distance from

center, i.e. increase in strain, did not contribute to grain refinement but changed its grain boundary misorientations as shown in figure 2-3. The distribution of crystal orientation was shifted to high angle even if the grain size did not change. In addition, the distribution of the most severely deformed sample area which was deformed with 5 rotations at the region 4 mm away from center (γ=210) was close to a random distribution calculated in a completely randomly oriented set of grains [17] as shown in figure 2-3 (a) as red line except for low angle regime due to limitations of EBSD measurement [18].

Inverse pole figures for normal direction of the disk obtained by EBSD analysis are shown in figure 2-4. Around 150 of the grains were analyzed in each, and showed preferred <110> orientation with respect to the normal direction of HPT processed disks in all specimens with different strain amount.

Evolution of microstructure by HPT process was observed during refinement of the grains until finest grain size in the specimen of γ=31 reached 300 nm in diameter. Saturation of grain refinement has been reported [19,20,21] with present results which saturation value is in 21 to 31 shear strain amount, i.e. equivalent strain amount of 15 to 22. Saturation grain size of HPT processed iron

reported has range from 250 nm to 100 nm [22,23]. Measured grain size will varies with evaluation method. FIB analysis or SEM backscatter image used in some reports depict grain and subgrain morphologies while present evaluation represents only grains with misorientation above 15 degrees. Moreover, in our EBSD analysis, grains smaller than 5 data points which corresponds to 60 nm in diameter were disregarded as error, which will cause over estimation of grain size. However, EBSD analysis using field emission SEM with step size 10 times larger than mean grain size will give enough accuracy for grain size measurement with less than 10 % error [18]. Grain boundary distribution shift was observed even after the onset of microstructural steady state, which indicates the occurrence of dynamic recrystallization during HPT process. This is consistent with previously reported TEM images showing the mixture of grains with high and low dislocation density [24]. During HPT process, initial grains are shear strained to the circumferential direction of the disk, and geometrically necessary dislocations are introduced to divide them into subgrains. Misorientation angle of the subgrain boundary increases as strain is introduced and turned into high angle nature. Owing to high dislocation density and small grain size, recrystallization of the grains could occur spontaneously during SPD process.

2.3.2 Compression test

Figure 2-5 (a), and (b) show SEM images of the micro-pillars before and after compression test. Parallel side walls of as-fabricated pillar clearly show no tapering in the specimen which is favorable for acquiring precise experimental data [25]. As widely accepted, pillar fabrication with irradiation from top of the pillar could cause a tapering geometry [26]. In the compression test with tapered pillar, stress is not uniform since cross-section area increased from top to bottom of the pillar. 10 % of compressive strain led to a few barreling of the sample. It was expected since friction between pillar top and diamond tip was relatively high (no lubricant used in this test) and the other end was fixed. This could affect the early stages of plastic deformation, until work softening caused by work hardening shortage was observed.

Figure 2-6 (a) shows a typical load displacement curve from micro-compression test. Tested pillar was fabricated at 4 mm away from center of the disk with 5 rotations of HPT resulted in shear strain amount of 210. Pillar was fabricated from the thin plate mounted on the holder, which gives relatively low

stiffness in the compression test and it varies with the thickness of the thin plate. In order to evaluate plastic deformation in compression test, elastic response was subtracted using yield point determined by 0.5% offset stress. The total strain after yielding can be represented as the sum of elastic and plastic compressive strains as $\varepsilon_{tot}=\varepsilon_e+\varepsilon_p$. Then if volume conservation law was assumed during plastic deformation, plastic contribution; ε_p can be estimated using following equation:

$$\varepsilon_p = \varepsilon_{tot} - \varepsilon_e = \frac{L}{L_0} - \frac{P}{EA_0} \qquad (1)$$

where P and L are the instantaneous load and displacement after yielding in compression test, E is the slope of load displacement curve in elastic section, A_0 and L_0 are the original cross-section area and height of the pillar (compressive stress is taken to be positive here).

The stress values were calculated by dividing the measured load by the original cross-section area; A_0. Calculated stress and strain were converted into true stress and strain respectively, then plastic true stress-strain graph was generated as shown in figure 2-6 (b). Fabricated pillar with SPD shear strain amount of 210 reached compressive stresses of 1.5 GPa. Results of pillar with different HPT conditions tested by micro-compression test were summarized in figure 2-7. The

pillar fabricated at 2 mm away from center of 1 rotated disk has the lowest stress of 1340 MPa and the others had around 1500 MPa. These results are expected because the grain size reached saturation at 30 of shear strain amount by HPT process and agrees well with hardness evaluation by Mine and Horita [27]. Further straining only changes its grain boundary characteristics but not affecting the strengths.

Work hardening rate; Θ is given by the following equation:

$$\Theta=\Delta\sigma/\Delta\varepsilon_p \qquad (2)$$

Figure 2-8 is the generated work hardening curve using 40 data points each, which corresponds to the very short, 1.2 sec, period of micro-compression test for calculation of work hardening rate. This continuous decrease in work hardening rate is responsible for the limited work hardening capacity. On the contrary, the coarse grain counterpart has linear strain hardening after yielding. There is notable difference in work hardening capacity in figure 2-8a and 2-8b with HPT strains of 21 and 210 respectively. As a good approximation, plastic instability is satisfied at a value of strain where the true stress equals the work hardening. Then,

$$\Theta \leq \sigma \qquad (3)$$

this formula is known as a Considere's criterion [27]. On the basis of this criterion, uniform elongation was determined with true plastic – true stress curves as open symbols in figure 2-8 and summarized in figure 2-9. Uniform elongation first decreased as decreasing grain size and increased while grain size and ultimate strength did not altered. On the contrary to our results, Mine et.al observed scattered elongations to failure and ultimate strength in miniature tensile test of the sample with strain amount of γ=73 [29]. Highest strength observed in miniature tensile test had similar value with our compression test. In the miniature tensile test, only slight scratches on the sample surface cause early failure of the specimens.

As mentioned in section 1, decrease in grain size was not observed in elongation of the metal with grain size less than 1 μm, and this is believed to be caused by early failure in tensile test [10,11]. On the other hand, our micro-compression test clarified that the uniform elongation is decreased with decreasing grain size. Work hardening mainly achieved by the accumulation of dislocations; however, UFG metals have a limited capacity to store dislocations owing to its tiny grains. It can be easily understood from expected decrease in work hardening capability due to lack of dislocation accumulation site. Elongation should be decreased not only with the

decrease in work hardening capability, but also with the increase in flow strength as proposed in Eq. (3). One should be noted from work hardening rate curve in figure 2-8, the difference in magnitude of the decrease in work hardening rate is almost the dominant factor for decrease in elongation. Therefore, work hardening is the key factor to achieve high strengths and large elongation simultaneously. In UFG materials, grain boundaries could be an effective dislocation accumulation site and its ability to store dislocation is highly dependent on the nature of grain boundary [1,8,9]. Grain boundaries in UFG materials subjected to SPD process often called non-equilibrium grain boundaries. Such boundaries have excess grain boundary energy, long range elastic stresses and free volume at the boundaries [1,7]. These features make it difficult for dislocation to accumulate at the grain boundaries and lead to limited work hardening. In a dynamic recrystallization, newly generated grains could have equilibrium grain boundary which randomly misoriented to the adjacent grains. This is a possible reason for increase in uniform elongation after microstructural saturation as shown in figure 2-9. Shift in misorientation angle indicates gradual transition of grain boundary from non-equivalent to equivalent boundary which can store much more dislocation.

2.4 Conclusion

In this work, micro-compression pillar was fabricated using two angles of ion irradiation. Fabricated pillar was not tapered and had 20 μm of square cross-section. EBSD analysis was performed in specific area with different strain amount. For ultra-low carbon ferrite, initial grain size of 300 μm were decreased to 300 nm at a shear strain amount of above 30, and further straining caused change in grain boundary misorientation distribution shifting to the high angle. This represents a dynamic recrystallization during SPD process. Micro-compression test clarified strength and ductility of HPT processed materials at specific area of interest. Strengths increased with increasing HPT strains or decreasing grain size and reached to 1.5 GPa of compressive strengths. Work hardening behavior after yielding showed rapid decrease in all tests. However, evaluated uniform elongation using Considere's criterion clarifies the decrease in elongation even in a sub-micron grain size regime. Increase in elongation after microstructural saturation was explained by gradual change in grain boundary misorientation which related to dynamic recrystallization in SPD process. Observed effect of grain boundary character on mechanical properties is very important for the UFG materials which has high fraction of grain boundary area.

2.5 References

[1] R.Z. Valiev, R.K. Isamgaliev, I.V. Alexandrov, Prog. Mater. Sci., 45 (2000) 103.

[2] Z. Horita, D.J. Smith, M. Furukawa, M. Nemoto, R.Z. Valiev, T.G. Langdon. J. Mater. Res., 11 (1996) 1880.

[3] R.Z. Valiev, T.G. Langdon, Prog. Mater. Sci., 51 (2006) 881.

[4] Y. Saito, H. Utsunomiya, N. Tsuji, T. Sakai, Acta Mater., 47 (1999) 579.

[5] R. Z. Valiev, V. Yu. Gertsman, O. A. Kaibyshev, Phys. Stat. Sol., (a), 57 (1986) 11.

[6] O.V. Mishin, V.Y. Gertsman, R.Z. Valiev, G. Gottstein, Scripta Mater., 35 (1996) 873.

[7] X. Sauvage, G. Wilde, S.V. Divinski, Z. Horita, R.Z. Valiev, Mater. Sci. Eng. A, 540 (2012) 1.

[8] R.Z. Valiev, F. Chmelik, F. Bordeaux, G. Kapelski, B. Baudelet. Scripta Metall. Mater., 27 (1992) 855.

[9] Y.H. Zhao, T. Topping, J.F. Bingert, J.J. Thornton, A.M. Dangelewicz, Y. Li, W. Liu, Y.T. Zhu, Y.Z. Zhou, E.J. Lavernia, Adv. Mater., 20 (2008) 3028.

[10] C.Y. Yu, P.W. Kao, C.P. Chang, Acta. Mater., 53 (2005) 4019.

[11] N. Tsuji, Y.Ito, Y. Saito, Y. Minamino, Scripta Mater., 47 (2002) 3.

[12] A. Vorhauer, R. Pippan, Scripta Mater., 51 (2004) 921.

[13] M.D. Uchic, D.M. Dimiduk, J.N. Florando, W.D. Nix, Science, 305 (2004) 986.

[14] Y. Todaka, M. Umemoto, A. Yamazaki, J. Sasaki, K. Tsuchiya: Mater. Trans., 49 (2008) 7.

[15] Y. Todaka, M. Umemoto, A. Yamazaki, J. Sasaki, K. Tsuchiya: Mater. Trans., 49 (2008) 47.

[16] G. P. Zhang, K. Takashima, Y. Higo, Mater. Sci. Eng. A, 426 (2006) 95.

[17] F.J. Humphreys, M. Matherly, *Recrystallization and related annealing phenomena*. Pergamon Press, Oxford, 1995.

[18] F. J. Humphreys, J. Mater. Sci., 36 (2001) 3833.

[19] A, A. Vorhauer R. Pippan, Metall. Mater. Trans., 39A (2008) 417.

[20] F. Wetscher, R. Pippan, Phil. Mag., 86 (2005) 5867.

[21] R.Z. Valiev, Y.U.V. Ivanisenko, E.F. Rauch, B. Baudelet, Acta Mater., 44 (1996) 4705.

[22] Y. Mine, Z. Horita, Y. Murakami , Acta Mater., 58 (2010) 649.

[23] S. Descartes, C. Desrayaud, E.F. Rauch, Mater. Sci. Eng. A, 528 (2011) 3666

[24] Y. Todaka, H. Nagai, Y. Takubo, M. Yoshii, M. Kumagai, M. Umemoto, Int. J. Mat. Res., 100 (2009) 775.

[25] H. Zhang, B.E. Schuster, Q. Wei, K.T. Ramesh, Scripta Mater., 54 (2006) 181.

[26] M.D. Uchic, D. Dimiduk, Mater. Sci. Eng. A, 400 (2005) 268.

[27] Y. Mine and Z. Horita, Mater. Trans., 53 (2012) 773

[28] G.E. Dieter, *Mechanical Metallurgy*, McGraw-Hill, Boston, MA, 1986.

[29] Y. Mine, S. Matsumoto, Z. Horita, Corros. Sci., 53 (2011) 2969

2.6 Tables

Table. 2-1. Calculated grain size from EBSD data at different area of HPT processed materials.

number of rotations	distance from center of the disk	shear strain amount	grain size
1	2 mm	21	510 nm
1	3 mm	31	290 nm
1	4 mm	42	290 nm
5	4 mm	210	300 nm

2.7 Figures

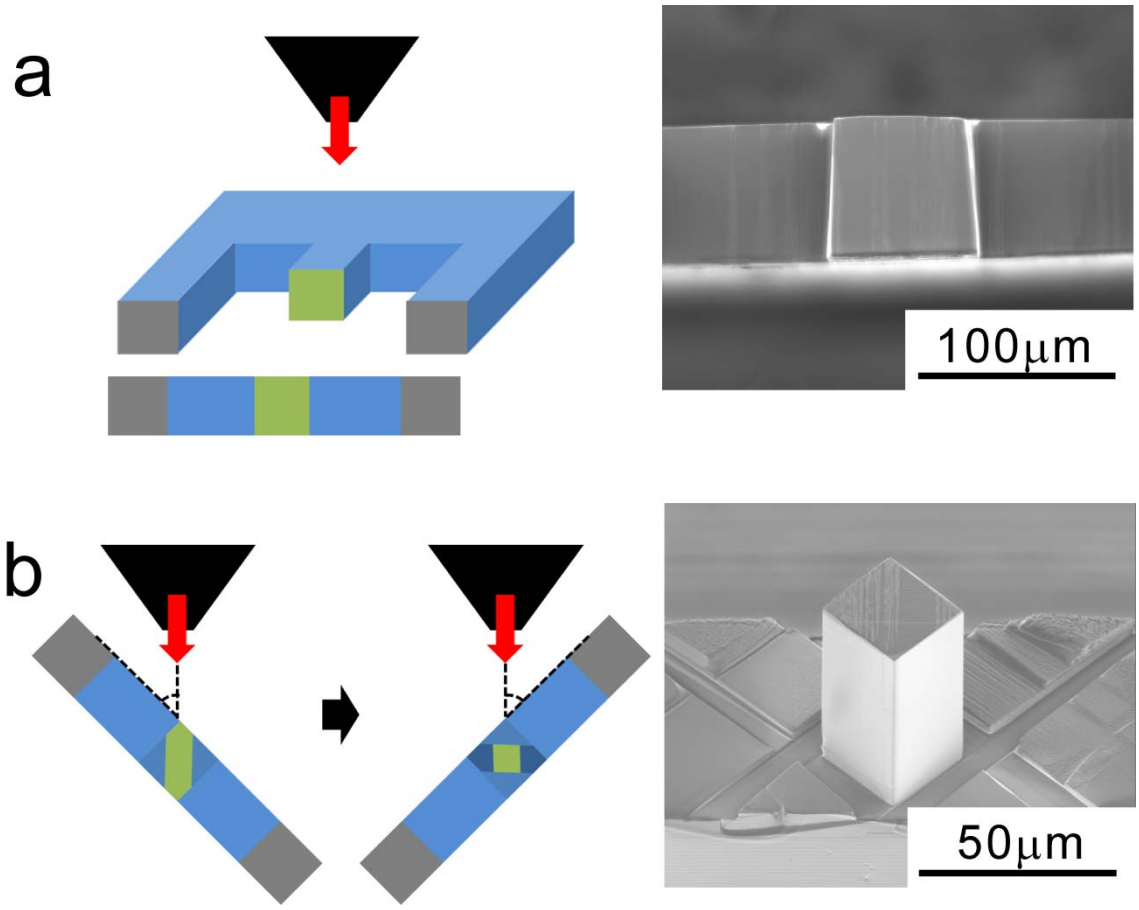

Figure 2-1. Procedures of making compression pillar and SIM images showing the pillar after the procedures: (a) perpendicular irradiation and (b) irradiation from 45 degrees from thin plate.

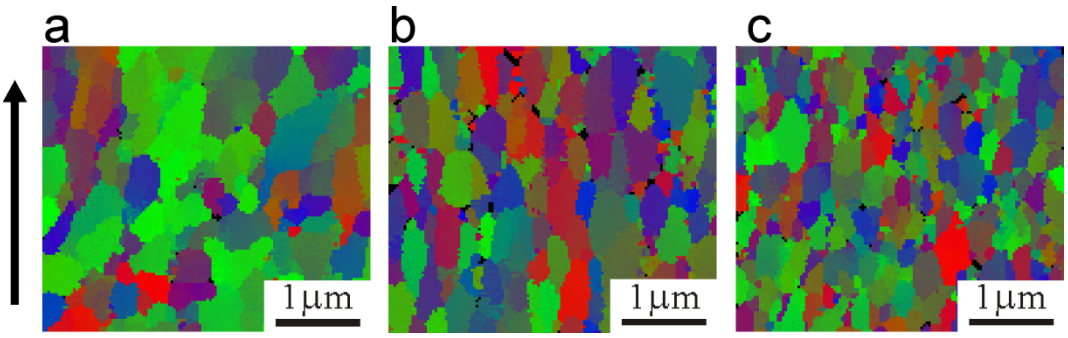

Figure 2-2. EBSD orientation maps of HPT processed ferrite with different shear strain (a) γ=21, (b) γ=42, and (c) γ=210. Arrow indicates shear direction in HPT process.

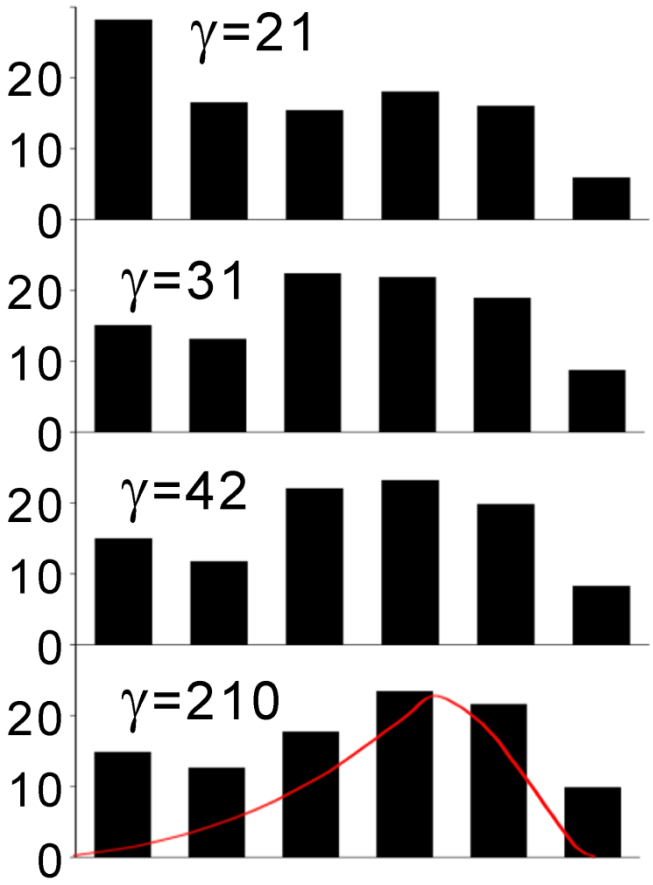

Figure 2-3. Grain boundary misorientation distributions obtained by EBSD analysis.

Red curve shows distribution of randomly oriented polycrystalline materials.

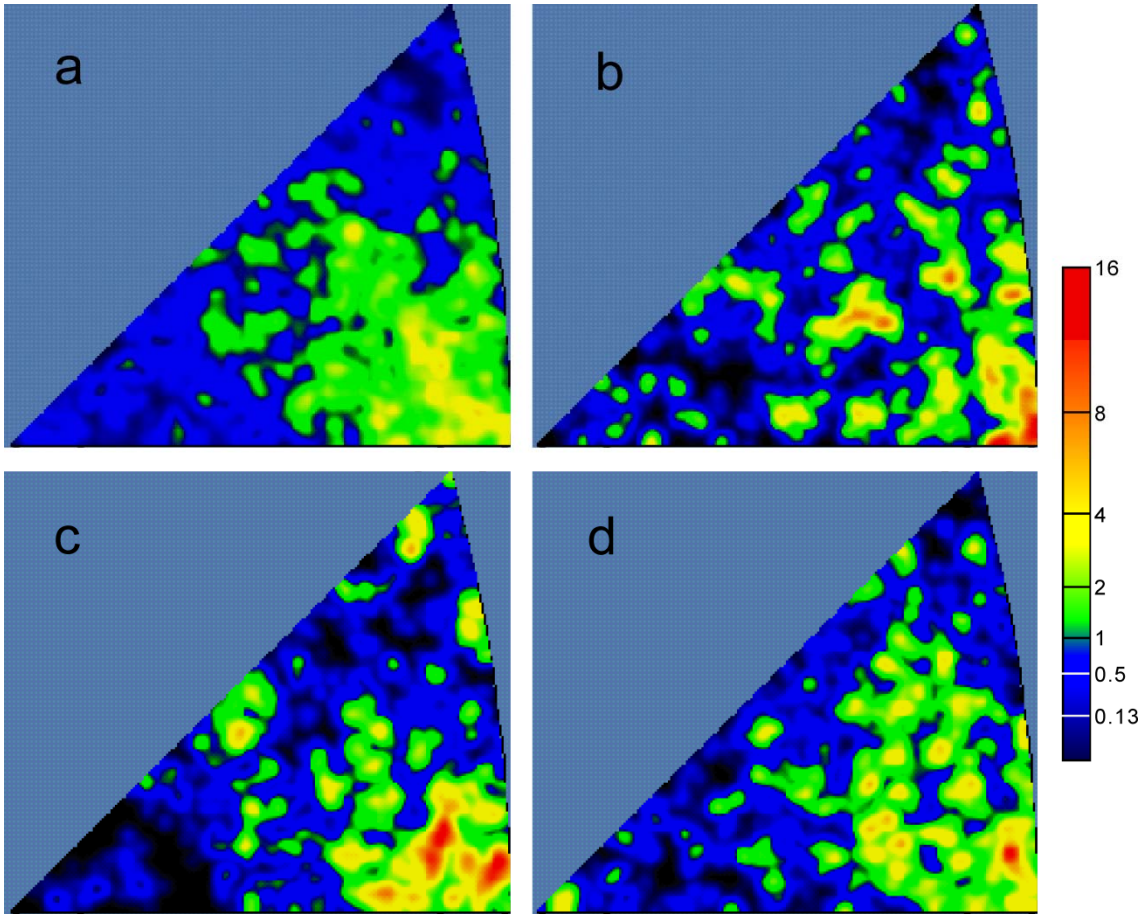

Figure 2-4. Inverse pole figure shows preferred orientation normal to the HPT disk where the shear strain with (a) γ=21, (b) γ=31, (c) γ=42, (d) γ=210.

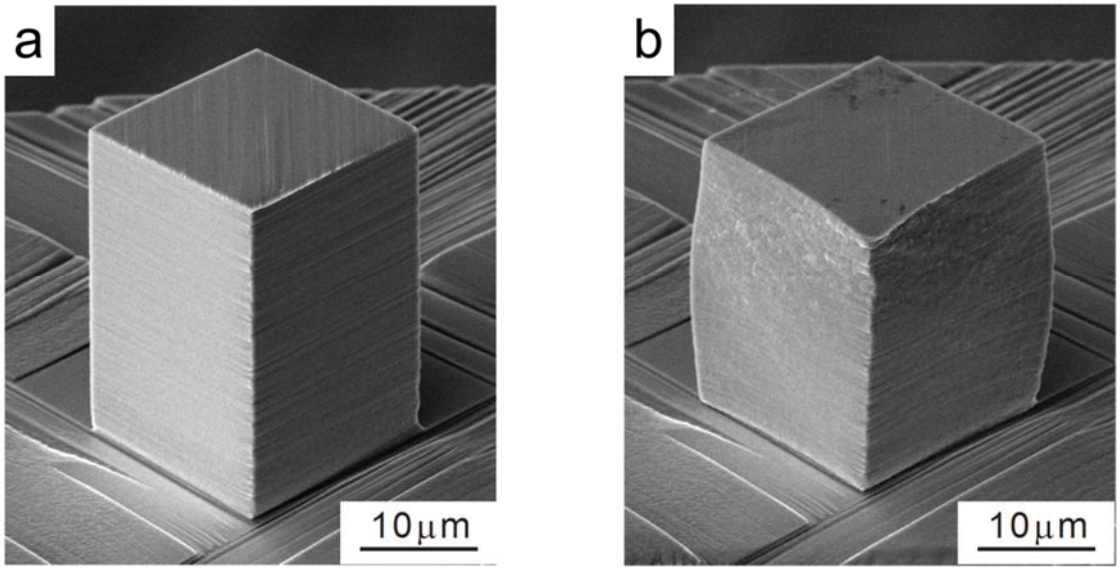

Figure 2-5. Representative SEM images of fabricated pillar (a) before and (b) after compressive deformation.

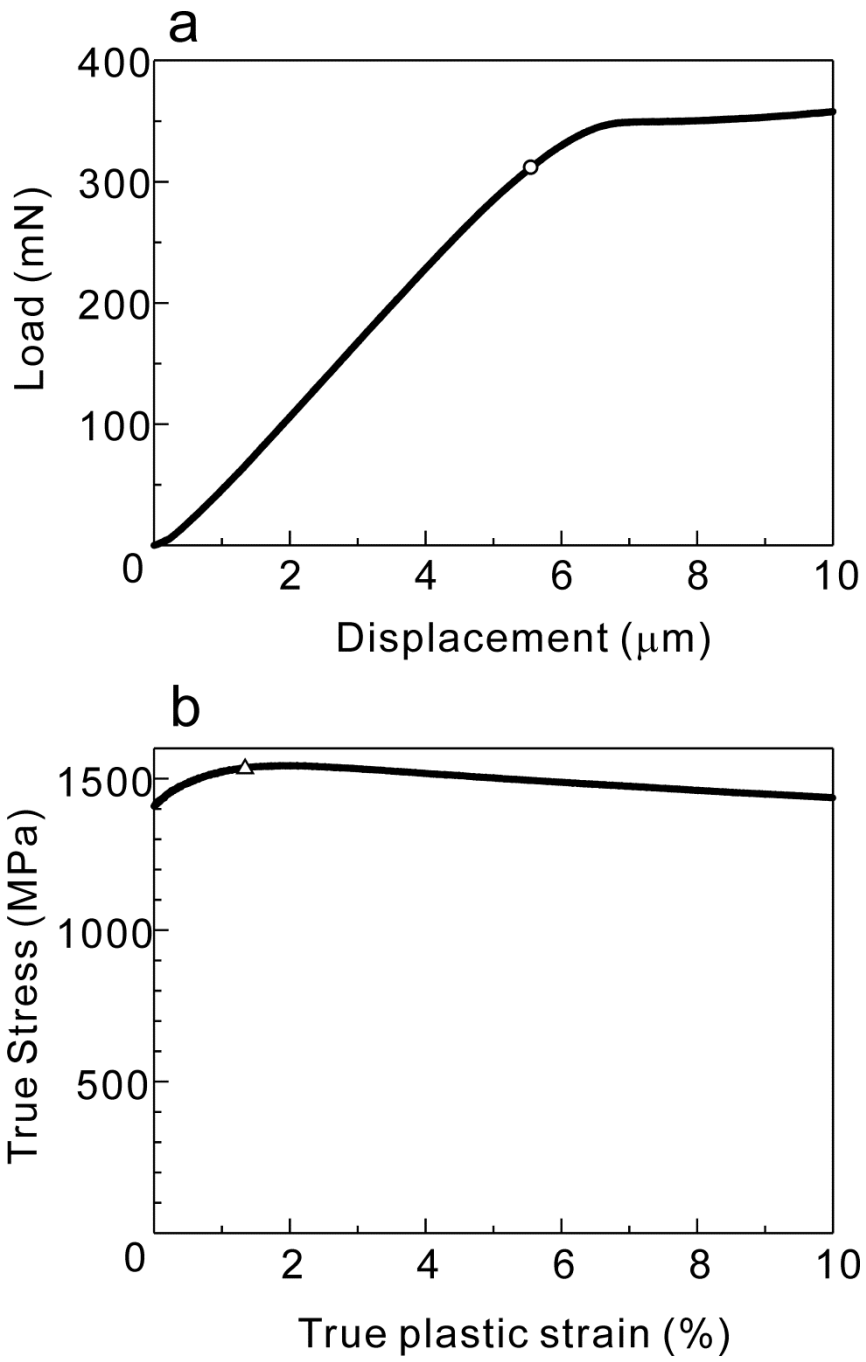

Figure 2-6. (a) Micro-compression test of a fabricated pillar, and (b) Plastic true stress-strain curves generated using the data in (a). Open triangle in (a) indicates 0.5 % offset stress.

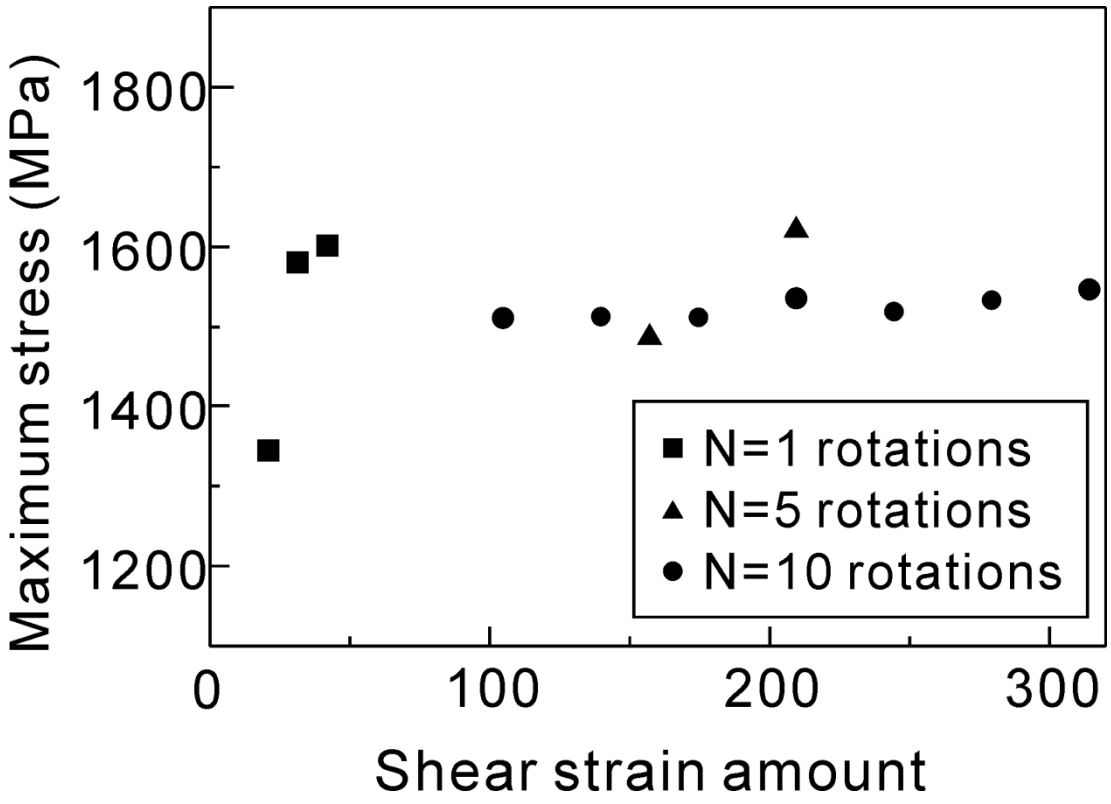

Figure 2-7. Observed maximum stress in micro-compression test vs. shear strain amount in HPT process of tested pillar.

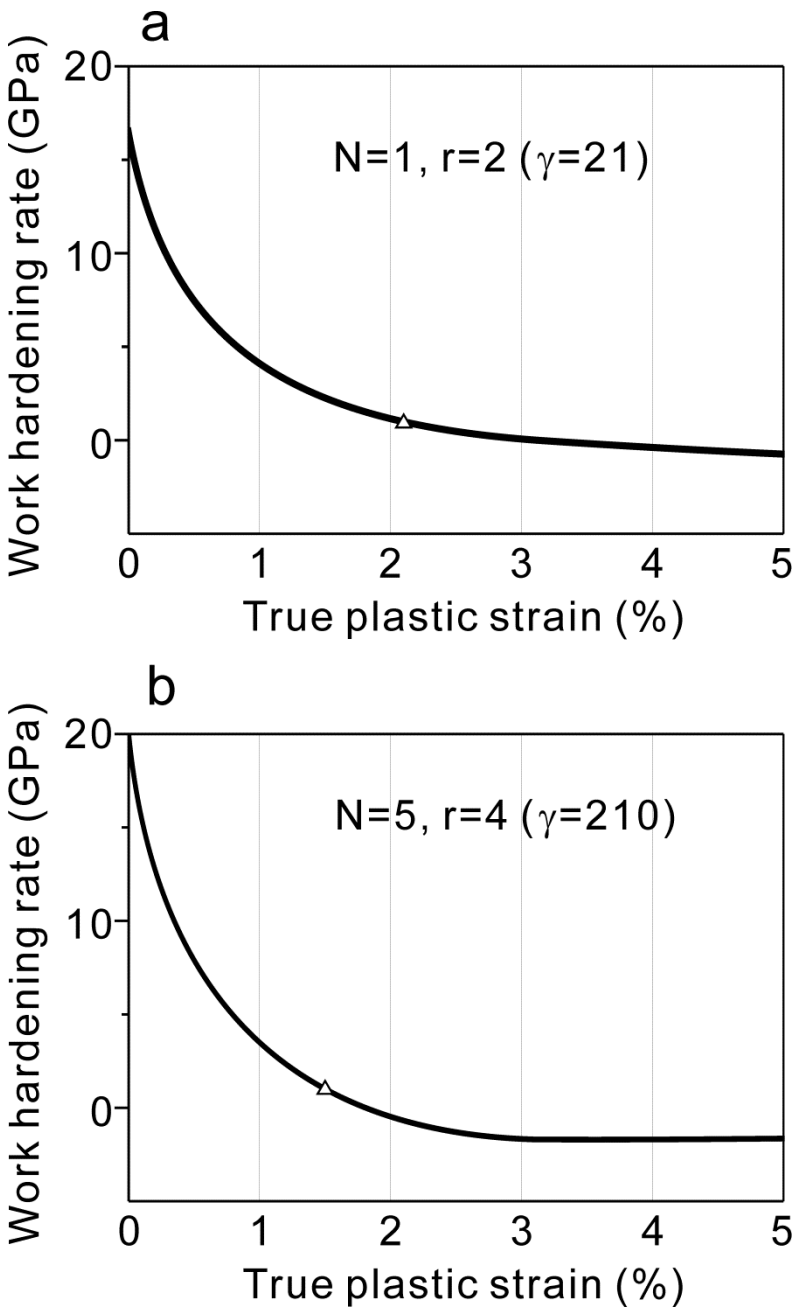

Figure 2-8. Work hardening rate curves generated from plastic true stress-strain curves of micro-compression test. Open triangle indicate uniform elongation (see text for explanation).

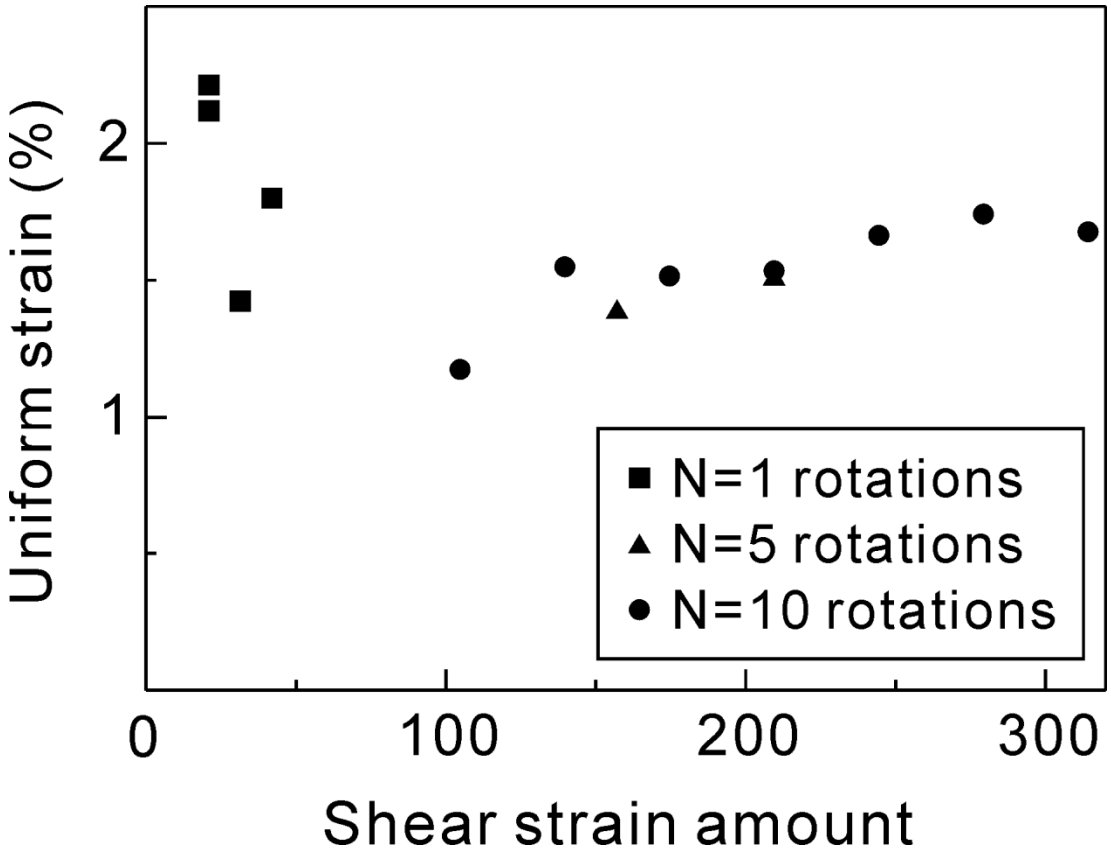

Figure 2-9. Uniform elongation in micro-compression pillar with different shear strain amount in HPT process.

CHAPTER 3

Mechanical properties of copper electrodeposited with supercritical CO_2 emulsion

3.1 Introduction

Copper materials are used for various electric devices because of the superior electric and thermal conductivity. Electrodeposition is an important technology for fabrication of micro-components used in MEMS devices [1,2] and related packaging technologies, such as copper wiring damascene process [3]. Especially for fabrication of three-dimensional structures, electroplating is an important process for miniaturization and densification of the microelectronics [4]. The Semiconductor Industry Association's International Technology Roadmap for Semiconductors predicts that half pitch of dynamic random access memory become 15.9 nm in 2018 [5]. However, voids and pinholes found in the electrodeposited copper of the integrated device can cause problems for the miniaturized device. Several studies have reported that different type of additives can be used to attain defect-free nano-scale copper filling [6-9]. However, further studies show that increase in

impurity concentration is observed with increase in usage of the additives, and impurity can cause serious problems for electric devices, such as increased electric resistance [10].

To solve these problems, our group has proposed a novel electroplating system, which is ESCE [11,12]. Merits of applying supercritical fluid are its high diffusivity, solubility and low surface tension. Agitation with surfactant enables an electrolyte and supercritical CO_2 to form emulsions with C/W type micelles. Critical point of CO_2 is relatively low (304 K and 7.39 MPa) when compared with other solvents, which make it a widely used in the industries and research area. In addition, CO_2 is non-polar, which can promote desorption of hydrogen gas bubbles from the surface of cathode. Adsorption of H_2 gas bubbles on the surface of cathode is reported to be one of the causes for defects found in electrodeposited films [13]. In previous study, we confirmed that these features given in ESCE can increase the quality of the plated film, such as film smoothening, and defect- and pinhole-free [14]. In addition, ESCE attained defect-free copper filling with nano-scale hole test element group [15].

However, effects of the supercritical CO_2 emulsion on the plated copper film electroplated by ESCE, especially microstructure and mechanical property, have not

been well studied. In the case of copper wiring or applications in MEMS, not only electrical property but also mechanical property is important. Characterizing the small-scaled and scale-specific mechanical properties of materials can provide design guidelines for reliable nano- and micro-electromechanical devices and developing models of the mechanical behavior of multicomponent structural materials. Therefore, we evaluated mechanical property of the copper films by micro-compression test using a non-tapered micro-sized pillar with square cross-section, which is fabricated from the plated films using FIB. We also observed film texture and measured impurity concentrations in the films by GDOES.

3.2 Experimental

3.2.1 Materials

CO_2 with purity of 99.99% purchased from Nippon Tansan Co. Ltd. was used. As a cathode and an anode in electrodeposition, High purity copper plate and Pt plate with 2.0×1.0 cm^2 were used respectively. Copper-sulfate-based electrolyte for conventional electroplating (CONV) was prepared based on previous report [16]. Electrolyte bath for supercritical CO_2 emulsified electrolyte was consisted of

copper-sulfate-based electrolyte with a composition of $CuSO_4$ (0.85 mol/L) and H_2SO_4 (0.55 mol/L) with 4.5 mL/L of Top Lucina α-M, 0.1 vol% of Top Lucina α-2, 0.3 vol% of Top Lucina α-3 (Okuno Industry Co. Ltd.), and 1 mmol/L of Cl^- (NaCl, Okuno Industry Co. Ltd.). As a surfactant, 1.0 vol% of polyoxyethylene lauryl ether [$C_{12}H_{25}(OCH_2CH_2)_{15}OH$], was added for formation of the emulsion.

3.2.2 Electroplating

Copper substrates were treated for 1 min in 10 wt% degreasing solution purchased from Okuno Industry Co. Ltd. Then, substrates were rinsed with distilled water. After that, substrates were treated for 10 sec in 10 wt% HCl, purchased from Okuno Industry Co. Ltd. Finally, substrates were again rinsed with distilled water. In the reaction cell before electroplating reaction, the emulsion composed of the aqueous electrolyte, the surfactant and supercritical CO_2 was stirred at 500 rpm for 10 min at 15 MPa to ensure stabilization of the emulsion [15]. Then, the electroplating reaction was conducted at 2.0 A/dm^2. Microstructure of the copper film was observed with FIB and SEM equipped with EBSD detector. Impurity content in the plated film was analyzed using GDOES (Rigaku: GDA750).

3.2.3 Micro-compression tests

Micro-sized pillars were fabricated using FIB (FB2100: HITACHI). Stress from top to bottom of the pillar is not uniform when tapered pillar is used in compression test, since the cross-sectional area increased from top to bottom of the pillar. Thus, non-tapered micro-pillar is required to obtain actual stress-strain curves. FIB induced Ga^+ ion damage on copper was studied by Kiener et al. [17]. They reported that the ion irradiation can increase more than 100 MPa in stress for samples with submicron dimensions when solid solution hardening by the penetrated Ga^+ ion and Taylor hardening by introduced dislocations were considered. However, it would be negligible for our samples with 20 μm on a side. Figure 3-1 shows schematic diagrams of the micro-pillar fabrication procedures by FIB and SEM image of the fabricated copper pillar. The procedures for non-tapered micro-pillar fabrication was reported in detail elsewhere [16,18].

The FIB fabricated pillars had 20 μm on a side with square cross-section and 40 μm in height. The compression tests were conducted using a test machine designed for micro-sized specimen [19]. Loading directions were parallel to copper film/substrate interface. Flat-ended diamond indenter equipped with load cell was

used as a compression platen, and controlled at a constant displacement rate of 0.1 μm/s using piezo-electric actuator. Force and displacement were recorded at every 33 milliseconds.

3.3 Results and discussion

3.3.1 Microstructure of copper films

Figure 3-2 shows FIB images of copper film electrodeposited. Different microstructure observed between as-deposited and two months after storage in a vacuum at room temperature. Observed grain size of copper films was about 0.1 μm in as-deposited and 1 μm after two months of storage and showed a similar structure to the as-deposited CONV copper. This significant microstructure evolution at room temperature called self-annealing was reported by many researchers [20]. There is no evidence but it is very possible that the self-annealing occurred in CONV case. Similar features of ESCE after self-annealing and CONV supporting this assumption. For the comparison of grain boundary structure, orientation maps were obtained by EBSD analysis as shown in figure 3-3. Grain boundary characteristics were also similar between self-annealed ESCE and CONV with large fractions of twin

boundaries. Fractions of high and low angle grain boundary with misorientation angle above 15 degree and between 5 and 15 degrees, respectively and special boundaries are tabulated in Table 3-1. These similarities in grain boundary structure and characteristics support the self-annealing phenomenon occured in both ESCE and CONV. The grain size of as deposited ESCE copper was finer than that of CONV. This grain refinement has been reported in ESCE nickel plating [18] and the main reason of refinement considered as follows; agitation with surfactant enables an electrolyte and supercritical CO_2 to form emulsions with C/W type micelles beyond critical pressure and temperature. C/W micelles could continuously bounce on the surface of working electrode while electroplating is in process, which gives periodic plating characteristic where the electroplating reaction is turned off when the surface of working electrode is in contact with the micelles and turned on when the micelles go away from the surface. And then, the grain growth is suppressed [14]. Our group reported that carbon concentration in the nickel film obtained by ESCE was higher than CONV's one [18]. Carbon impurity will be works as a barrier for grain growth in self-annealing. Hence, we discuss the impurity concentration in the electrodeposited copper film in the next section.

3.3.2 Impurity in electrodeposited copper

GDOES analysis was used for evaluation of impurity concentration inside film. Figure 3-4 shows carbon concentrations in the copper films. The depth represents the distance from the film surface, and both concentration peaks were at the interface between film and substrate calculated from deposition time and current densities. Observed peak at the surface was considered to be because of contamination of the film surface. Similar carbon distribution in CONV and ESCE copper film indicates that the carbon impurity derives from identical source. In both electrolytes, additives such as suppresser, accelerator and leveler were used. These additives adsorbed at substrate and involved into the film during electroplating reaction. Impurity element of O which believed to derive from oxidation had also been observed and shown in figure 3-5. Broad small peak observed at the interface responsible for remained oxidized layer in pretreatment. Both impurities were observed as same levels in the film deposited by ESCE and CONV. Thus, the results confirmed that the electroplating method of ESCE would not cause additional contamination problems in the plated copper film.

3.3.3 Mechanical properties evaluated by micro-compression test

Figure 3-6 shows true stress-strain curve of copper pillars fabricated from the films of as-deposited and two months after ESCE and CONV. A significant difference is observed in mechanical strength between as-deposited ESCE and CONV. Engineering stress of the as-deposited ESCE pillar was about 300 MPa higher than CONV pillar. And strength decreased by self-annealing to the same level of CONV pillar. Deformation behavior is very similar in both self-annealed ESCE pillar and CONV pillar well agreed to the identical microstructure observed. There is linear work hardening regime in compression test of CONV pillar and self-annealed ESCE pillar, but not observed in compression test of as-deposited ESCE pillar. Figure 3-7 shows SEM image of pillars after the compressive deformation. In the copper pillar of CONV, many slip traces can be observed on the surface at the individual grains. Therefore, the deformations can be assumed to occur as dislocation activation inside grains. On the contrary, sharp shear band crossing through the pillar observed in as-deposited ESCE pillar, which explains no linear hardening in compressive deformation. SEM images from different side in figure 3-8 indicating

the shear sliding of pillar top. Decrease in cross sectional area followed by shear localization responsible for the work softening lather than work hardening behavior in micro-compression of as-deposited ESCE. This is because the dislocation storage is strikingly limited by grain refinement when the grain size is in sub-micron meter regime.

Besides limited work hardening, strength was increased in as-deposited ESCE pillar compared to self-annealed ESCE and CONV pillar. The main reason of strengthening is considered to be a grain refinement strengthening. It is widely accepted that grain refinement strengthening is explained as a shortage of dislocation pile-up length due to decreased distance between grain boundaries. This strengthening contribution formulated by Hall and Petch known as H-P relationship as following;

$$\sigma = \sigma_0 + kd^{-\frac{1}{2}} \qquad (1)$$

σ, σ_0, and k are yield strength, friction stress and the constant for the material, respectively. We calculated increase in yield strength with equation (1) when grain size decreases from 1.0 to 0.1 μm. When we refer constant k (MPa・$m^{0.5}$) as 0.14 in previous report on copper [21]. The calculated increase in strength was about 300

MPa. This is in good agreement with experimental results of this study. Hence, copper pillar of as-deposited ESCE can be explained only by grain refinement of ESCE. Considering the results of GDOES, grain refinement strengthening should be the main factor contributing to increase of mechanical strength.

3.4 Conclusion

Effects of copper electroplating method of ESCE and CONV on the mechanical properties were investigated using micro-compression. The results presented here allow the following conclusions to be made.

The grain size of the plated copper by ESCE became finer than that by CONV. The grain size was reduced from 1.0 to 0.1 μm for CONV and ESCE, respectively. However, due to the self-annealing of ESCE copper, after the storage of 2 months results in the structure change to the almost same features of grain size and grain boundary characteristics of CONV copper.

Impurity concentrations in the copper films were almost same in both ESCE and CONV and have a peak at the interface between substrate and plated film. Impurities of carbon and oxygen suggested to be derived from additives adsorbed on

the surface of substrate before electroplating and involved at an early stage of electrodeposition.

A significant increase in strength of as-deposited ESCE copper was observed ESCE and CONV, and strengths of the Cu pillar deposited by ESCE was about 300 MPa higher than that by CONV. H-P type strengthening fully explains increased strength and further softening to the same stress level of CONV copper which has similar grain structures.

Finally, the presented features of ESCE fabricated copper film which showed high initial strength and further softening by recrystallization without any treatment indicates great possibility of this plating method to apply copper wiring damascene process. Initial high strength imply the reduced failure in packaging process and further grain growth can improve conductivity even for extremely small process rules.

3.5 References

[1] M. Gad-el-Hak, *The MEMS Handbook*, CRC, Taylor & Francis, Boca Raton, Florida, 2006.

[2] D.T. Read, Y.W. Cheng, R. Geiss, Microelectron. Eng., 75 (2004) 63.

[3] P.C. Andoricaco, C. Uzoh, J.O. Dukovic, J. Horkans, H. Deligianni, IBM J. Res. Dev., 42 (1998) 567.

[4] O. Luhn, A. Radisic, C.V. Hoof, W. Ruythooren, J.P. Celis, J. Electrochem. Soc., 157 (2010) D242.

[5] Semiconductor Industry Association, *2011 International Technology Roadmap for Semiconductor*, Semiconductor Industry Association, Incheon, Korea, 2011.

[6] T.P. Moffat, D. Wheeler, M. Edelstein, D. Josell, IBM J. Res. Dev., 49 (2005) 19.

[7] W.P. Dow, M.Y. Yen, W.B. Lin, S.W. Ho, J. Electrochem. Soc., 152 (2005) C769.

[8] A.C. West, S.T. Mayer, J. Reid, Electrochem. Solid State Lett., 4 (2001) C50.

[9] T.P. Moffat, J.E. Bonevich, W.H. Huber, A. Stanishevsky, D.R. Kelly, G.R. Stafford, D. Josell, J. Electrochem. Soc., 147 (2000) 4524.

[10] T. Osaka, N. Yamachika, M. Yoshino, M. Hasegawa, Y. Negishi, and Y. Okinaka, Electrochem. Solid State Lett., 12 (2009) D15.

[11] H. Yoshida, M. Sone, H. Wakabayashi, H. Yan, K. Abe, X.T. Tao, A. Mizushima, S. Ichihara, S. Miyata, Thin Solid Films, 446 (2004) 194.

[12] H. Yoshida, M. Sone, A. Mizushima, H. Yan, H. Wakabayashi, K. Abe, X.T. Tao, S. Ichihara, S. Miyata, Surf. Coat. Tech., 173 (2003) 285.

[13] W.L. Tsai, P.C. Hsu, Y. Hwu, C.H. Chen, L.W. Chang, J.H. Je, M.H. Lin, A. Groso, G.Margaritondo, Nature, 417 (2002) 139.

[14] T.F.M. Chang, M. Sone, Surf. Coat. Tech., 205 (2011) 3890.

[15] N. Shinoda, T. Shimizu, T.F.M. Chang, A. Shibata, M. Sone, Microelectron. Eng., 97 (2012) 126

[16] M. Mutoh, T. Nagoshi, T.F.M. Chang, T. Sato, M. Sone, Microelectron. Eng., 111 (2013) 118.

[17] D. Kiener, C. Motz, M. Rester, M. Jenko, G. Dehm, Mater. Sci. Eng. A, 459 (2007) 262.

[18] T. Nagoshi, T.F.M. Chang, T. Sato, M. Sone, Microelectron. Eng., 110 (2013) 270.

[19] A. Shibata, T. Nagoshi, M. Sone, Mater. Sci. Eng. A 527 (2010) 7538.

[20] M. Stangl , J. Acker, S. Oswald, M. Uhlemann, T. Gemming, S. Baunack, K. Wetzig, Microelectron. Eng., 84 (2007) 54.

[21] A.W. Thompson, W.A. Backofen, Metall. Trans., 2 (1971) 2004.

3.6 Tables

Table 3-1. Fractions of special grain boundaries (%).

copper films	High angle GB	Low angle GB	Twin GB	Less than 45 sigma value CSL boundaries
2 months after ESCE	99.2	0.8	69.7	83.3
CONV	99.3	0.7	62.6	71.0

3.7 Figures

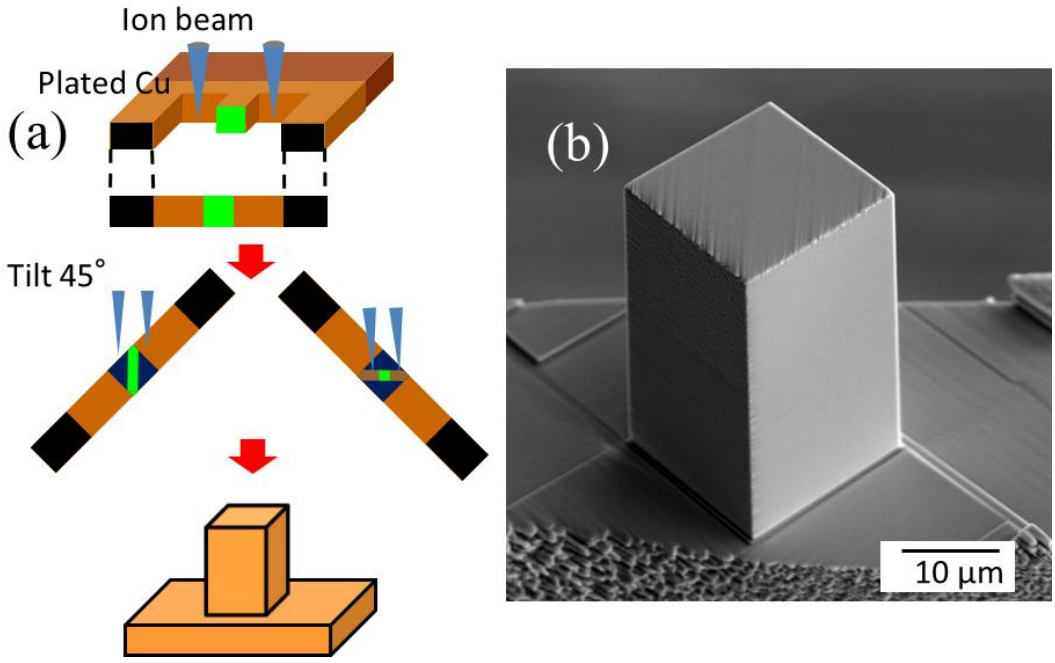

Figure 3-1. (a) Schematic image showing flow of the pillar fabricated with FIB, and (b) SEM image of the copper pillar fabricated.

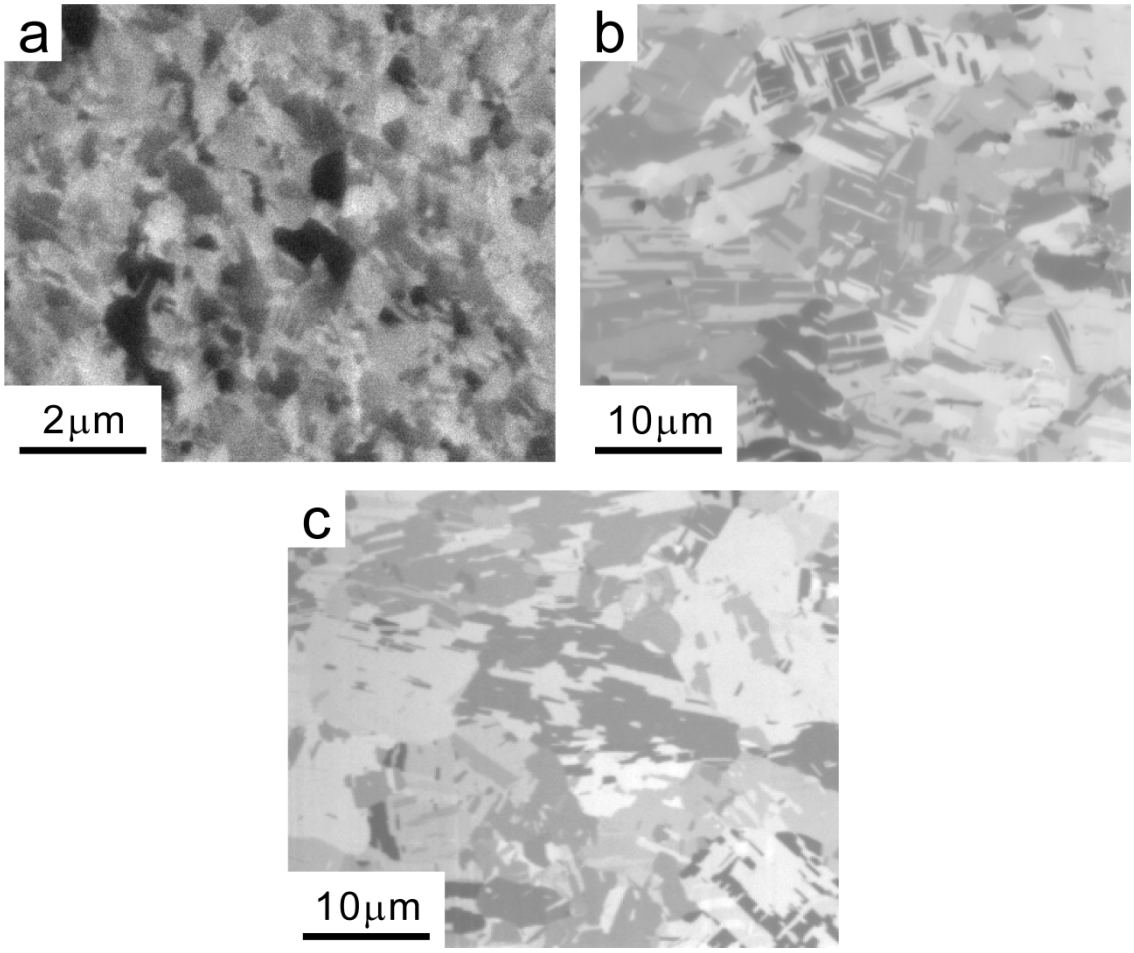

Figure 3-2. SIM images of copper film (a) as deposited ESCE , (b) two months after ESCE and (c) CONV plated.

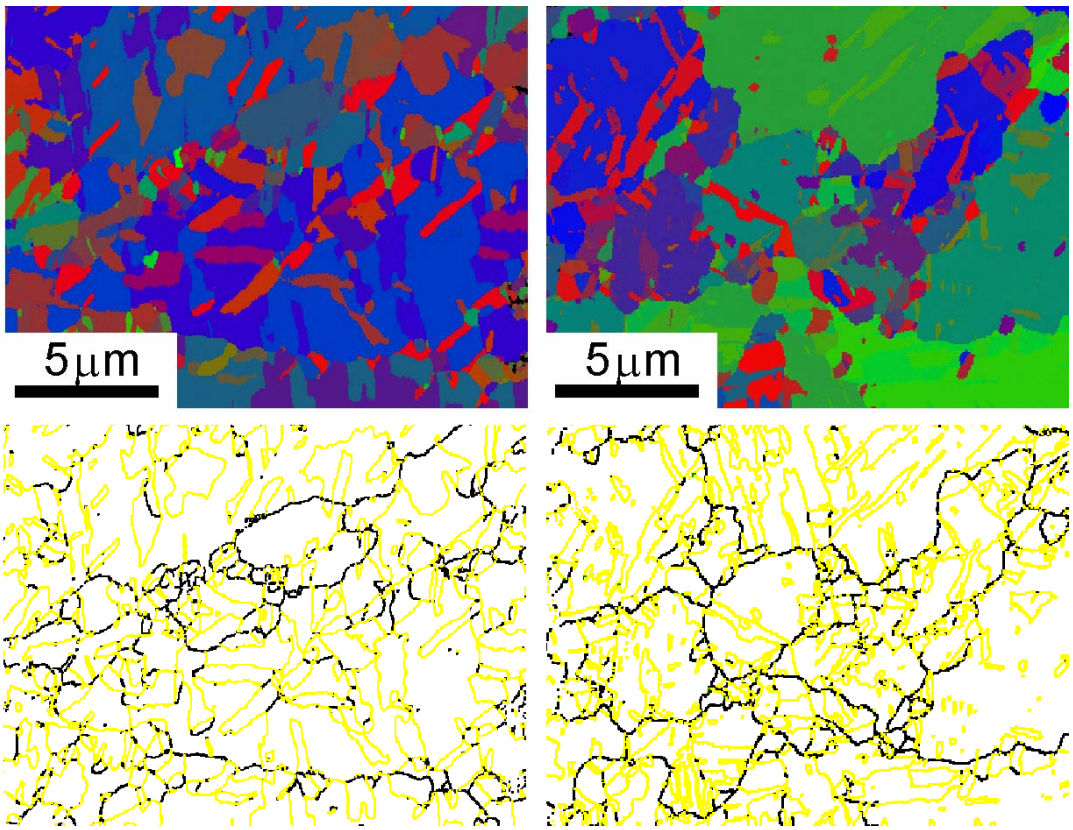

Figure 3-3. EBSD orientation maps of (a) ESCE after 2 months and (b) CONV copper film. Corresponding grain boundary map (c,d) showing high angle boundaries with misorientation angle above 15 degrees and twin boundaries denoted as black and yellow lines, respectively.

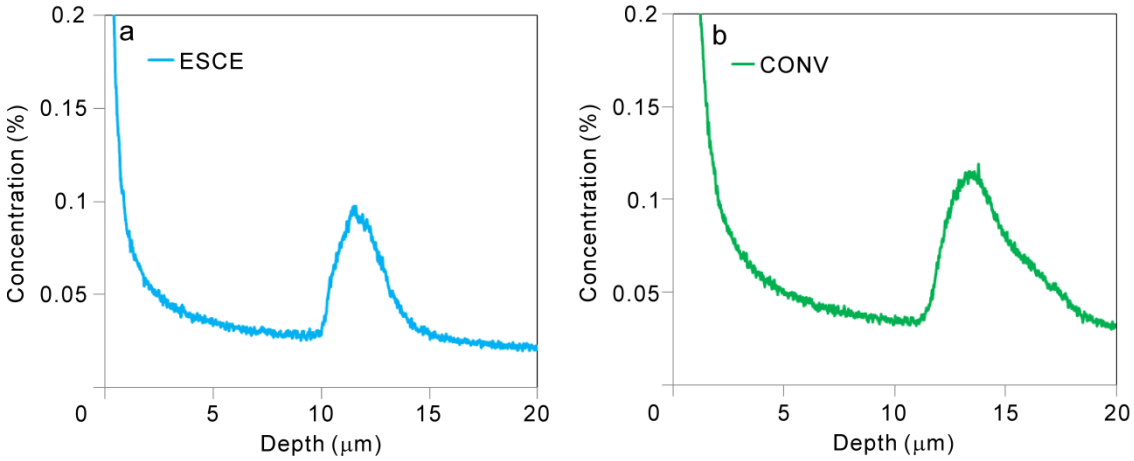

Figure 3-4. Carbon impurity concentrations in the copper film fabricated by (a) ESCE and (b) CONV observed using GDOES.

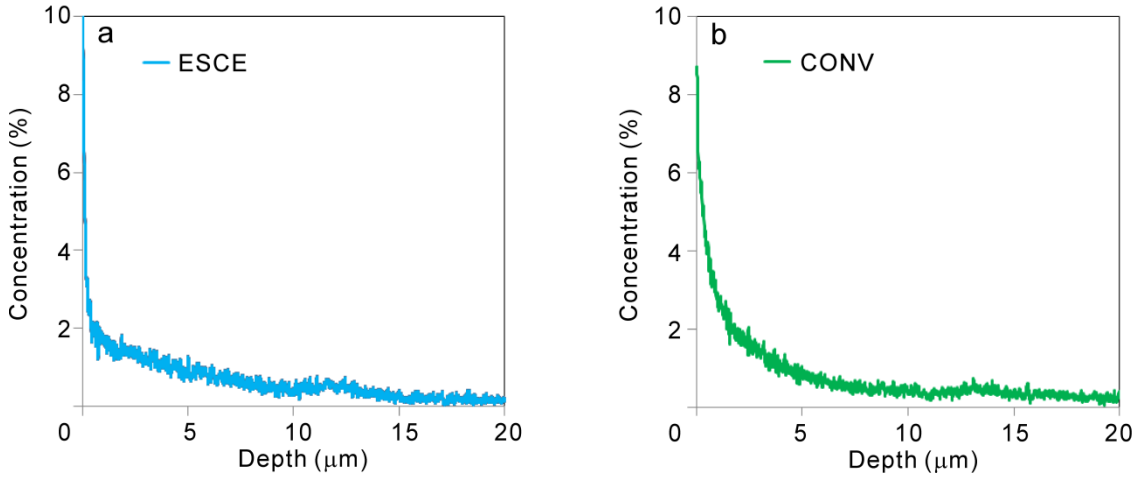

Figure 3-5. Oxygen impurity concentrations in the copper film fabricated by (a) ESCE and (b) CONV observed using GDOES.

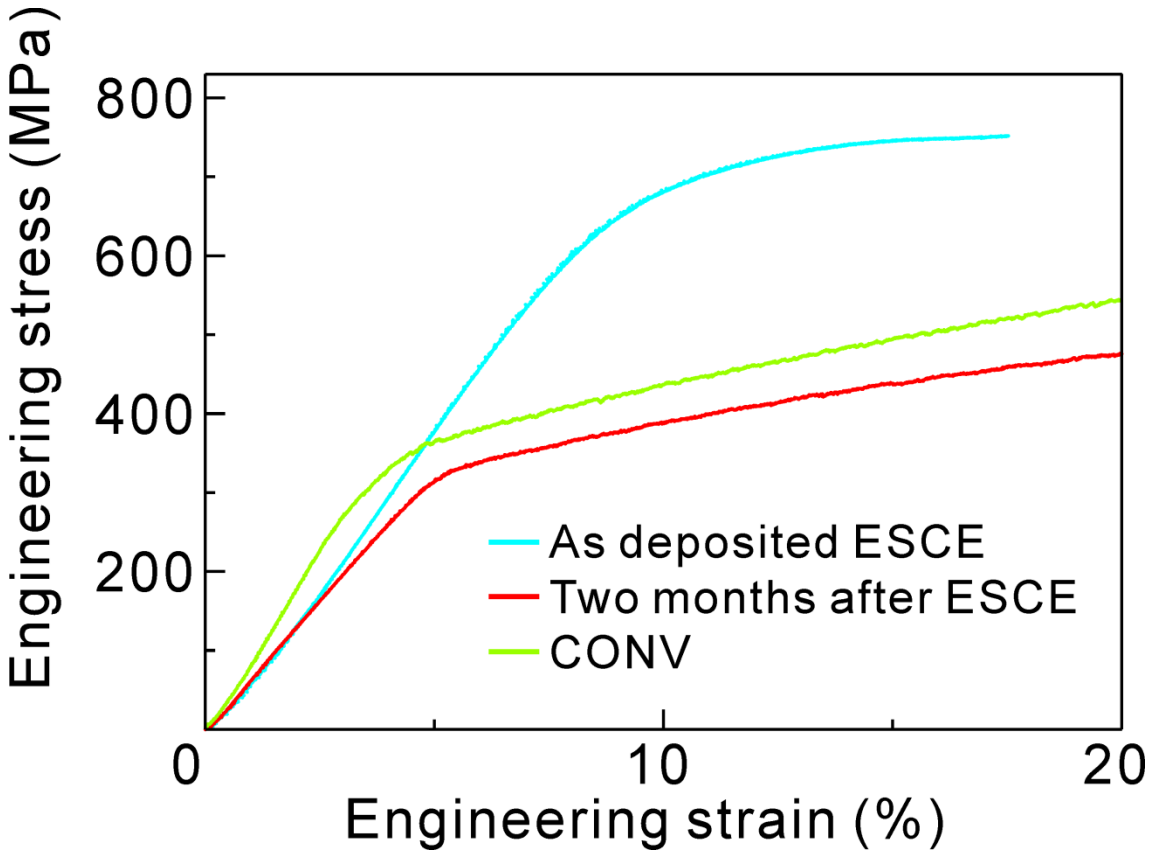

Figure 3-6. Engineering stress-strain curves in micro-compressions of pillars fabricated from as deposited ESCE copper film, two months after deposition of ESCE copper film, and CONV copper film.

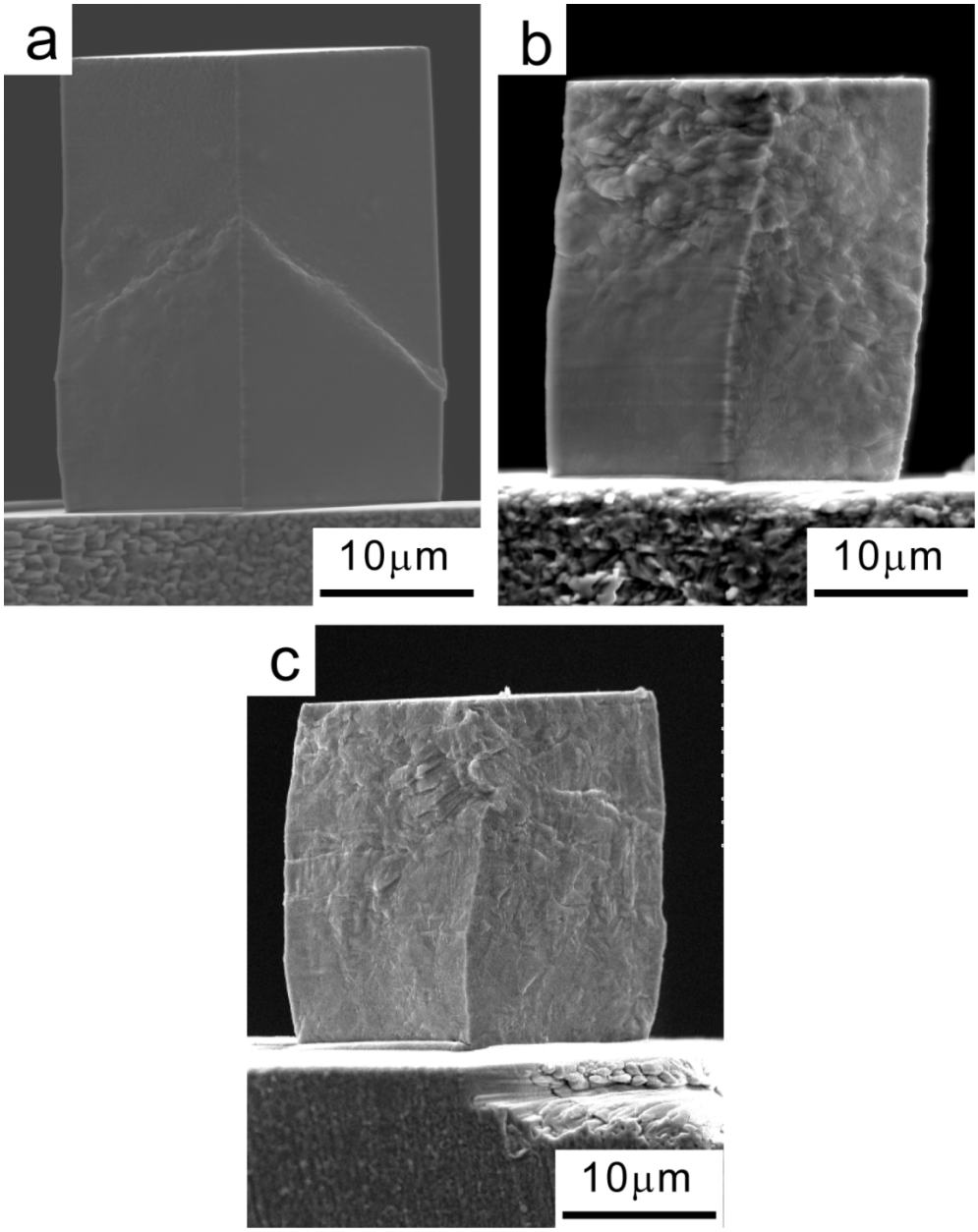

Figure 3-7. SEM images of post deformed copper pillar of (a) as-deposited ESCE, (b) two months after ESCE and (c) CONV.

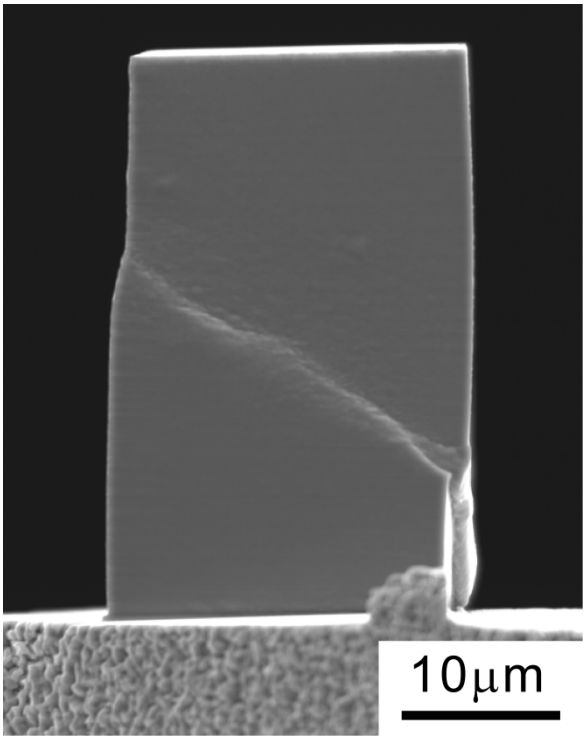

Figure 3-8. SEM image of as-deposited ESCE pillar taken from right side face of figure 3-7a.

CHAPTER 4

Mechanical properties of nickel electrodeposited with supercritical CO_2 emulsion

4.1 Introduction

Recently, micro-sized materials with high strength to be used as mechanical components in MEMS are required for development of MEMS. Electroplating is a good candidate to fabricate micro-components used in MEMS [1]. Incorporating the electroplating method with lithography enables fabrication of metallic micro-patterns. Microstructures such as crystallographic orientations and grain size can also be easily controlled by changing pH of electrolyte [2], usage of additives [3] or pulse plating method [4] to meet the favorable mechanical properties of the components.

We have developed an ESCE. Agitation with addition of surfactant enables an electrolyte and supercritical CO_2 to form emulsions with CO_2-in-water (C/W) type micelles at a certain pressure and temperature [5]. C/W micelles could continuously bounce on the surface of working electrode while electroplating is in process, and which gives periodic plating characteristic (PPC). PPC is like pulse plating where the

electroplating reaction is turned off when the surface of working electrode is in contact with the micelles and turned on when the micelles go away from the surface. Hydrogen gas bubbles evolved as a side reaction of electroplating could be immediately engulfed by the micelles because of high solubility of hydrogen in CO_2. These features given in ESCE can increase the quality of the film plated, such as grain refinement, film smoothening, and defect- and pinhole-free plating [5]. The physical properties of supercritical CO_2, such as high diffusivity and low surface tension also contribute to the ESCE. Yan et al. reported when CO_2 is substituted by n-hexane for formation of the emulsion, the surface condition of the plated nickel films became worse [6]. Thus the properties of dispersion phase are important and can be varied by changing pressure.

In this work, effects of the supercritical CO_2 emulsion on the nickel films fabricated by ESCE, especially microstructure and mechanical property were examined. Mechanical properties were investigated by micro-compression test using a non-tapered micro-sized pillar with square cross-section. The micro-sized pillars were fabricated from the plated films by using focused ion beam (FIB) machine. This investigation examines the potential of the ESCE for applications in MEMS

fabrication by clarifying the microstructures and mechanical properties of the plated film with different applied pressure.

4.2 Experimental

4.2.1 Electroplating

Nanocrystalline nickel films were prepared by ESCE. Copper substrates were degreased and pre-treated with 10 wt% degreasing solution (Ace clean, Okuno Industry Co., Ltd) and 10 wt% HCl solution (Okuno Industry Co., Ltd), respectively. Pre-treated substrates were electroplated at a constant temperature of 323 K and different pressure of 6, 10, 15, 20 MPa applied by high-pressure experimental apparatus (Japan Spectra Company) shown in figure 4-1. A non-ionic surfactant, polyoxyethylene lauryl ether ($C_{12}H_{25}(OCH_2CH_2)15OH$) from Toshin Yuka Kogyo Co., Ltd. was used to emulsify the aqueous electrolyte and supercritical CO_2. Additive free Watts bath was used as an electrolyte which is composed of $NiSO_4 \cdot 6H_2O$ (50 g/l), $NiCl_2 \cdot 6H_2O$ (50 g/l), and H_3BO_4 (50 g/l). The reaction chamber was a 316 stainless steel cylinder coated by polyetheretherketone with an inner volume of 50 ml. The reaction chamber was filled with 20 vol.% of CO_2 with respect to the volume of the reaction chamber and 2.0 vol.% of surfactant with

respect to the volume of the aqueous electrolyte. A magnetic agitator with a cross-shaped magnetic-stirrer-bar placed in the reaction camber was used for mixing. Detailed set up of the apparatus can be found elsewhere [7]. Electroplating was performed on both sides of the copper substrate under constant current density of 2 A/dm^2.

4.2.2 TEM observation

TEM observation was conducted with JEM-2100F (Jeol) operating at acceleration voltage of 200 kV in bright field mode. TEM specimens were prepared by FIB with JIB-4500 (Jeol) using lift-out technique from film surface. Electroplated films were first coated with approximately 100 nm thick carbon by physical vapor deposition with E101 (Hitachi). A ~10 μm long by 5 μm wide by 5 μm deep trench was milled to isolate a 1 μm thick nickel plate. The plate is then lifted out via omniprobe attached with W to a custom made TEM lift out grid. Grid was made from half split single hole copper grid bridged with 1 μm thick Al film. This custom made TEM grid enables to do following argon ion milling with glancing angle irradiating from both side of TEM grid while standard TEM grid disturbs the pass of ion milling from one side which emphasize wedge shaped TEM specimen. For the

argon ion milling, Model1010 (Fischone) operating at 2 kV, 6 mA was used to ensure electron transparency with removal of Ga ion damaged layer.

4.2.3 Material evaluation

Structural characterization of plated films was performed by X-ray diffraction (XRD) using Ultima IV (Rigaku Instrument). The X-ray was generated by a copper target operated at 40 kV and 40 mA. The XRD profiles were used to confirm the crystal structures and lattice constants and to estimate the average grain size by Scherrer equation. Only (111) diffraction peak was used for the calculation. From a cross sectional areas of plated nickel using HPE, microstructure observation was conducted using scanning electron microscopy (SEM) by S-4300FE (Hitachi) equipped with electron backscatter diffraction pattern detector (EBSD, Oxford instruments: INCA Crystal software).Glow discharge optical emission spectroscopy (GDOES) with GDA 750 (Rigaku) was used to evaluate impurity content in the plated films. The depth profiles of containing elements were measured in RF mode (constant voltage-constant pressure mode) with the 500 V, 280 Pa. Obtained intensities from emission lines of interest, which are Ni (341.477 nm), Cu (327.396 nm), B (249.773 nm), C (156.143 nm), and O (130.217), were calibrated by standard

materials for quantitative analysis. Sputtering depth was calculated by measuring the sputtering area and mass of sputtered materials, considering the material density.

4.2.4 Micro-compression test

Electroplated substrate was sliced using electric discharge machine and mechanical polished. Compression pillar was fabricated from the edge of the sliced sample which is the prior surface of the electroplated film. FIB equipment FB2100 (Hitachi) operating at 40 kV was used to fabricate the pillar. Sequences of pillar fabrication using FIB are illustrated in figure 4-2. In the process of fabrication; first, a pillar with thickness of around 150 μm was fabricated, as shown in figure 4-2a. Then irradiation with incident angle of 45 degree from the thin plate was used to make a small pillar at the center of the bigger one as shown in figure 4-2b to avoid mechanically damaged area. Ion beam from side of the specimen allowed the fabrication of a pillar with uniform dimensions (non-tapered, non-filleted), which was favorable for acquiring precise experimental data. Due to usage of cone-shaped ion beam, which is commonly used and one of the main causes of tapering for FIB fabricated micro-pillar using one-directional irradiation [8], side face of the pillar was slightly tilted to beam direction. Finally, each side of the pillar at a tilt angle of ±2.3 degree was etched with 400 pA ion beam to minimize ion bombardment

damage (figure 4-2c). The pillars fabricated had 20 μm on a side with square cross-section and 40 μm in height. The critical dimensions of the gage length and cross-sectional area were measured by SEM for the conversion of the load and displacement data to a stress-strain curve.

Once the micro-compression pillars were fabricated, the samples were tested in uniaxial compression using a test machine designed for micro-sized specimen at room temperature. Loading direction was parallel to the copper substrate/nickel film interface. A flat-ended diamond indenter with 50 μm diameter equipped to piezoelectric actuator stage applies displacement to the specimen at a constant displacement of 0.1 μm/s which in turns strain rate of 0.003 s^{-1}.

4.3 Results and discussion

4.3.1 Microstructure

In plan-view TEM bright field image in figure 4-3a observed from nickel plated by ESCE at 15 MPa,. The areas of grain observed in TEM bright field images were measured by image-J software and the diameter of an equivalent circle having the same area defined as a grain size. Distribution of grain size electroplated at 15 MPa based on more than 500 grains measured from several TEM images shown in

figure 4-3b, where a very narrow grain size distribution from several nm to near 20 nm with near symmetric manner observed. Figure 4-4 shows average grain size of the films fabricated by ESCE at different pressure based on measurement of around 100 grains in TEM. Measurements by XRD and TEM showed similar trend and the TEM results are used as average grain size hereafter in this paper. Equi-axial grains were found in all samples viewed from sample surface and cross section. The smallest grain size of 8 nm was obtained in nickel film electrodeposited at 15 MPa. In the ESCE system, grain refinement is achieved by PPC due to the bouncing micelles. Density of the CO_2 inside micelles increases with increase in pressure especially near the transition point from gas to supercritical phase. Change in density of the dispersed phase in emulsion will have an effect on the micelle structure and dispersion conditions. Thus, the change in grain size by different applied pressure was expected.

4.3.2 Impurity concentrations

Compositions of film were summarized in the table 4-1 averaging the concentration depth profiles from 5 μm to 15 μm including nickel deposited with supercritical CO_2 but without surfactant thus the emulsion not formed. High level of

carbon impurities was found in electroplated nickel and shown in figure 4-5 as a depth profile of carbon atomic concentration. Results of GDOES from electrodeposited nickel by CONV with adding surfactant was included. Carbon concentration has peaks at the interface and slightly decreased with deposition process except for nickel deposited at 20 MPa. Comparing with CONV plated nickel without surfactant; some impurities derived from surfactant detected not only the surface but also inside the film. However, in the emulsified state, surfactant consumed by the formation of micelles and number of surfactant adsorbed and involved in film could decrease. Similar concentration levels of oxygen among CONV and ESCE plated films imply surfactant extinction at the surface while surfactant mainly composed of carbon and oxygen. Surfactant-free deposition also shows the same level of carbon included in the nickel deposition. These results showing the carbon derives from CO_2 dissolved in an electrolyte. Dissolution rate of CO_2 in water is increased with increasing pressure, which agrees well with the carbon concentration found in ESCE nickel. Carbon concentration in the nickel lattice as a solute can be estimated by the lattice expansion evaluated by XRD using following formula [9]

$$a=0.35447+0.00080c$$

while a is the lattice constant and c is the concentration of carbon dissolved as solute atom. Calculated carbon concentrations are shown in figure 4-6 including the averaged concentration shown in table 4-1. For ESCE nickel, about 2 at% of carbon present inside grains as a solute and the rest of the carbon, the difference in global concentration and intragranular concentration will segregate at grain boundaries. Wang et al. have reported the high binding energy of carbon impurity to nickel grain boundary [10], thus, the solute carbon could be easily segregate to the grain boundary.

4.3.3 Mechanical properties

Micro-compression test was conducted and the deformed pillars were observed as shown in figure 4-7. All the pillars were deformed by broad shear banding crossing through top to bottom. However, for the nickel film electrodeposited at 6 and 20 MPa, notable difference as bulging on the pillar surface was found as shown in figure 4-7a and 4-7c. These bulged areas were connected with small shear trace which along the broad shear band. This abnormal deformation morphology was observed in the film which has around 15 nm of grain size. Micro-compression test results are shown in figure 4-8 as true stress-true plastic strain curves. No clear relationships were found between deformation morphology

and stress-strain behavior. Highest maximum stress of 3500 MPa was observed in the film electrodeposited at 15 MPa which had smallest grain size of 8 nm.

As a discussion of strengthening, traditional solid solution strengthening should be considered where the solute atoms of carbon act as obstacles to dislocation motion. There are several theories for interpretation of solid solution strengthening in metals; however, for our dilute solid solution of carbon, Fleischer formulation [11] is sufficient to offer a correct number of strengthening effect by solute atom. In the Fleischer model, interaction parameter, ε_s, shear modulus, G, and solute concentration, c, were used to calculate increase in shear strength $\Delta\tau$ in following formula.

$$\Delta\tau = \frac{G \cdot \varepsilon_s^{\frac{3}{2}} \cdot c^{\frac{1}{2}}}{760}$$

Assuming the misfit parameter as a local change of lattice parameter aforementioned in the calculation of interstitial carbon concentration, $\Delta\tau$ as a function of the interstitial carbon concentration was shown in figure 4-9. Carbon interstitials found in ESCE nickel was around 2 at% and the estimated strengthening is 7.9 MPa in shear stress which can be negligible considering the present high maximum stress of 3500 MPa. In the following section, this outstandingly high strength was discussed based on H-P relationship.

4.3.4 Hall-Petch relationship

The influence of grain size on the strengths of metals and alloys has been studied extensively followed by early work of Hall [12] and Petch [13]. The extensive experimental data are in good agreement with the H-P equation

$$\sigma=\sigma_0+kd^{-0.5}$$

where d is the grain size, σ_0 is a friction stress and k is a constant called H-P intensity parameter [12]. However, recent experimental results sometimes showed opposite trend, called H-P breakdown in the materials with very small grain size. This is considered to be corresponded to the change in deformation mechanisms from dislocation mediated to grain boundary mediated such as grain boundary sliding [14], grain rotation [15], and grain boundary dislocation emission [16]. In such deformation mechanisms, Increased area fraction of grain boundary region gives softening of materials and a critical grain size with maximum strength has been found to be in the range of 10-20 nm depends on materials [17,18,19]

However, our nanocrystalline nickels obey H-P relationship until finest grain size of 8 nm. Strength of nanocrystalline nickel with grain size of 8 nm is on the extrapolated H-P slope from nickel alloy as shown in figure 4-10. One third of Hardness values of pure nickel [18,20,21] and Ni-W alloy [22] are included in H-P

plot assuming Tabor relation [23] as well as 0.2% yield stress in present micro-compression test. This suppression of H-P breakdown is consistent with a literature reported by Schuh et al. their hardness of Ni-W alloy has fallen in 8-9 nm and suggested that the alloying with tungsten has suppressed the H-P breakdown [22]. They concluded that the slow diffusion of tungsten in nickel increase required stress for activation of Coble creep and grain boundary sliding. Present electrodeposited nickel was reported to have 2.6 at% of global carbon concentration and 2.0 at% of intragranular carbon concentration, and the rest of the carbon could be segregated at the grain boundaries. On the contrary to the tungsten in nickel, carbon has very high diffusivities in nickel via interstitial site diffusion. Yin et al. reported an effect of interstitials on creep deformation via Coble creep and grain boundary sliding [24]. On that literature, interstitially dissolved atoms are reported to effectively enhance creep resistance. H-P breakdown represents a transition of deformation mechanism from dislocation mediated to grain boundary mediated. Thus, if the grain boundaries are reinforced by impurities, dislocation motion dominates the deformation at much smaller grain size and results in suppressed H-P breakdown.

4.4 Conclusion

Nanocrystalline nickel films were fabricated using ESCE at different applied pressure. PPC effect successfully refines the grains of plated film while the micelle properties varied by the applied pressure. The most effective PPC effect were attained at a pressure of 15 MPa and results in the smallest grain size of 8 nm. Micro-compressions of nickel film deposited by ESCE were conducted using non-tapered micro-pillar. Yield stress obeys H-P relationship along with the various nanocrystalline nickel and Ni-W alloy. Generally observed H-P breakdown at 10-20 nm was not observed in present nanocrystalline nickel with finest grain size of 8nm. This suppression of H-P breakdown explained by increased stress for grain boundary mediated deformation emergence due to enhanced grain boundary cohesion by impurity carbon. Our additive-free electroplating of ESCE could produce nanocrystalline nickel with grain size of 8 nm which has enhanced strength due to suppression of H-P breakdown.

4.5 References

[1] M. Gad-el-Hak, The MEMS Handbook (CRC, Taylor & Francis, Boca Raton, Florida., 2006)

[2] J. Amblard, I. Epelboin, M. Froment, G. maurin, J. Appl. Electrochem. 9(1979) 233-242

[3] A.M. Rashidi, A. Amadeh, Surf. Coat. Technol. 204 (2009) 353-358

[4] H. Wakabayashi, N.Sato, M. Sone, Y.Takada, H. Yan, K. Abe, K.Mizumoto, S.Ichihara, S. Miyata, Surf. Coat. Technol. 190 (2004) 200-205.

[5] T.F.M. Chang, and M. Sone, Surf. Coat. Technol. 205 (2011) 3890-3899.

[6] X. Yuan, Y. Wang, D. Sun, H. Yu, Surf. Coat. Technol. 202 (2008) 1895-1903.

[7] T.F.M. Chang, M. Sone, A. Shibata, C. Ishiyama, Y. Higo, Electrochim. Acta, 55 (2010) 6469.

[8] M.D. Uchic, D.M. Dimiduk, Mater. Sci. Eng. A, 400 (2005) 268.

[9] R.C. Ruhl and M. Cohen, Scripta Metall., 1 (1967) 73

[10] L.G. Wang, C.Y. Wang, Mater. Sci. Eng. A, 234 (1997) 521

[11] R.L. Fleischer, Acta Metall., 9 (1961) 996

[12] E.O. Hall, Proc. Phys. Soc. London B, 64 (1951) 747

[13] N.J. Petch, J. Iron Steel Inst., 174 (1653) 25.

[14] H.V. Swygenhoven, P.A. Dertret, Phys. Rev. B, 64 (2001) 224105.

[15] Z.W. Shan, E.A. Stach, J.M.K. Wiezorek, J.A. Knapp, D.M. Follstaedt, S.X. Mao, Science, 305 (2004) 654.

[16] Z. Budrovic, H.V. Swygenhoven, P.M. Derlet, S.V. Petegem, B. Schmitt, Science, 304 (2004) 273.

[17] P.G. Sanders, J.A. Eastman, J.R. Weertman, Acta Mater., 45 (1997) 4019.

[18] C.A. Schuh, T.G. Nieh, T. Yamasaki, Scripta Mater., 46(2002) 735.

[19] T.G. Nieh, J.G. Wang, Intermetallics, 13 (2005) 377

[20] F. Ebrahimi, G.R. Bourne, M.S. Kelly and T.E. Matthews, Nanostruct. Mater., 11 (1999) 343.

[21] G.D. Hughes, S.D. Smith, C.S. Pande, H.R. Johnson, R.W. Armstrong. Scripta Metall., 20 (1986) 93.

[22] C.A. Schuh, T.G. Nieh, H. Iwasaki, Acta Mater., 51 (2003) 431.

[23] D. Tabor, *The Hardness of Metals*, Oxford University Press, London, 1951.

[24] W.M. Yin, S.H. Whang, R.A. Mirshams, Acta Mater., 53 (2005) 383.

4.6 Tables

Table 4-1. Impurity concentrations of electrodeposited nickel film with various conditions

deposited film	Concentration (%)		
	Boron	Carbon	Oxygen
CONV	0.000785	0.015	0.027
CONV with surfactant	0.00564	0.46	2.54
ESCE at 6MPa	0.000910	1.91	0.0220
ESCE at 10MPa	0.00114	2.43	0.0355
ESCE at 15MPa	0.00114	2.61	0.0305
ESCE at 20MPa	0.00102	2.17	0.0153
Plated at 15MPa without surfactant	0.000961	2.20	0.0590

4.7 Figures

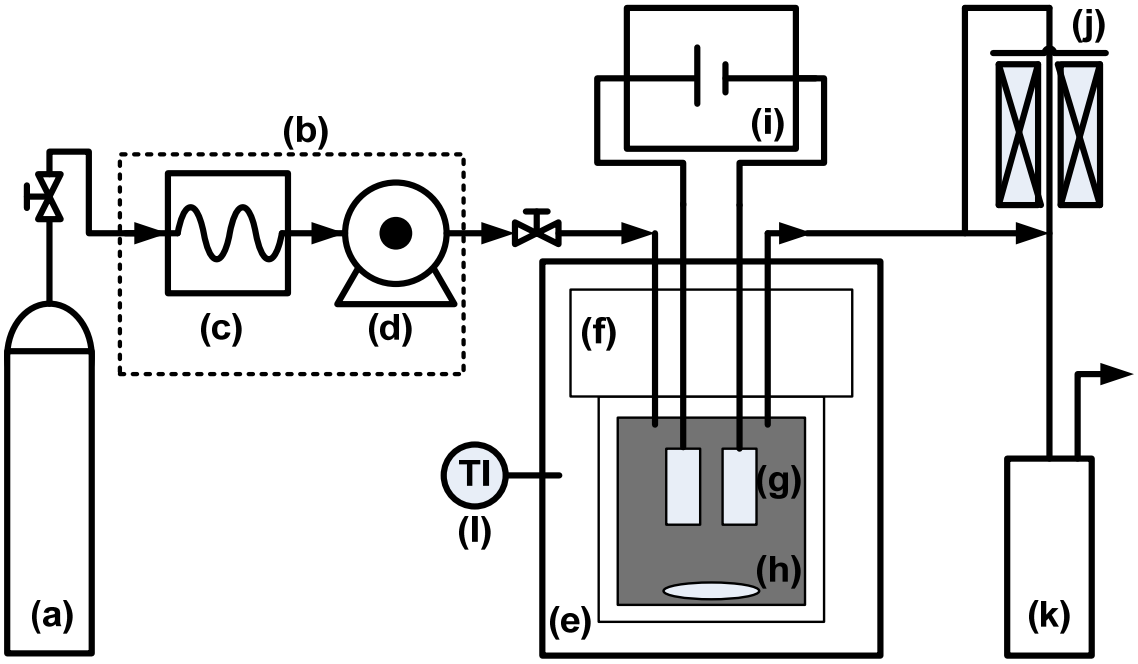

Figure 4-1. High pressure apparatus: (a) CO_2 gas tank, (b) CO_2 liquidization unit, (c) liquidization unit, (d) high-pressure pump, (e) thermal bath, (f) reaction cell, with PEEK coating on the inner wall, (g) electrodes, (h) stirrer, (i) programmable power supply, (j) back pressure regulator, (k) trap, (l) thermometer.

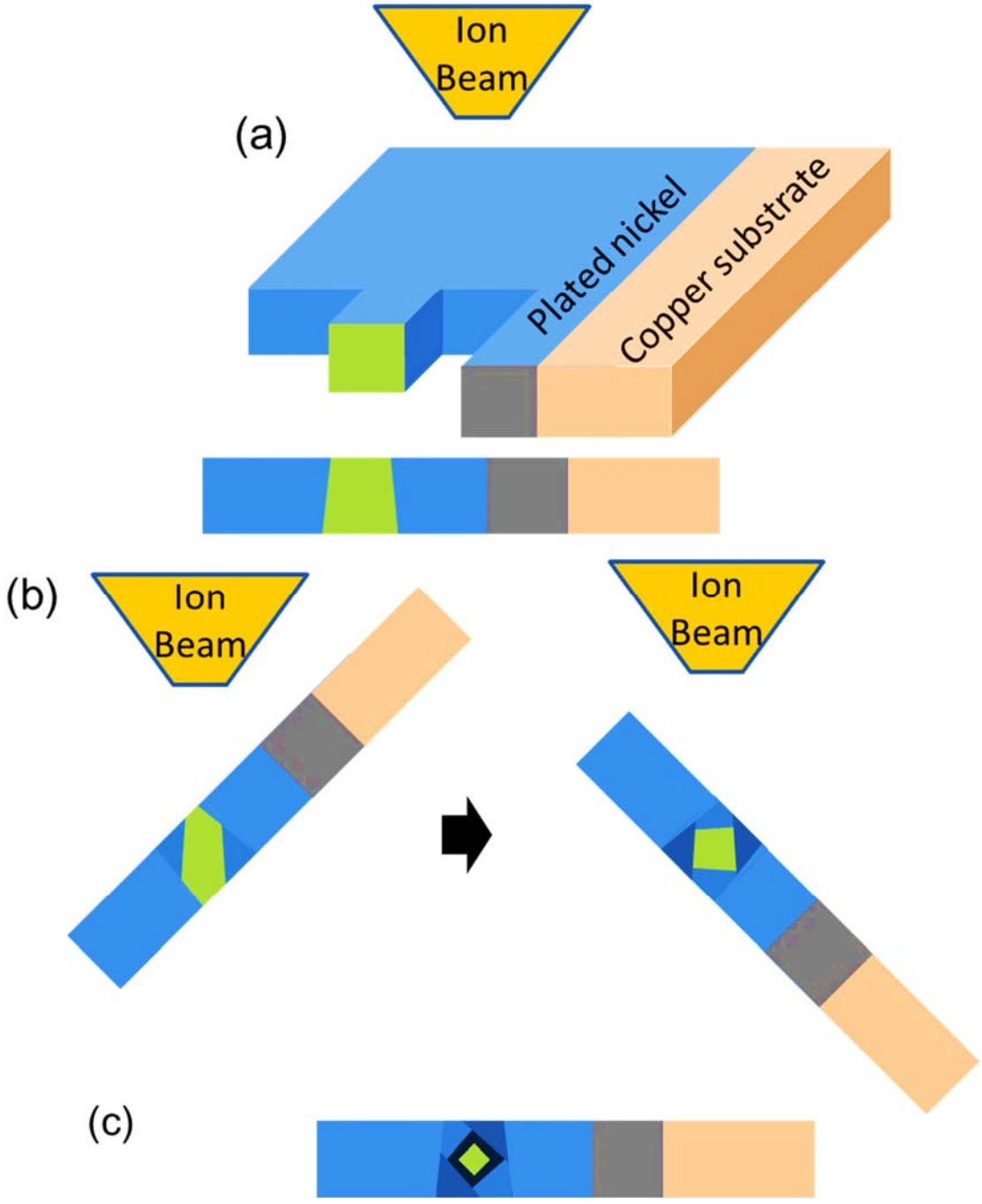

Figure 4-2. Schematic flow showing the sequences for fabrication of micro-compression pillar: (a) fabrication of the pillar with the size of thickness of sliced sample. (b) Size reduction of the pillar with irradiation at an incident angle of 45 degree. (c) Finishing with low current beam at a tilt angle of ±2.3.

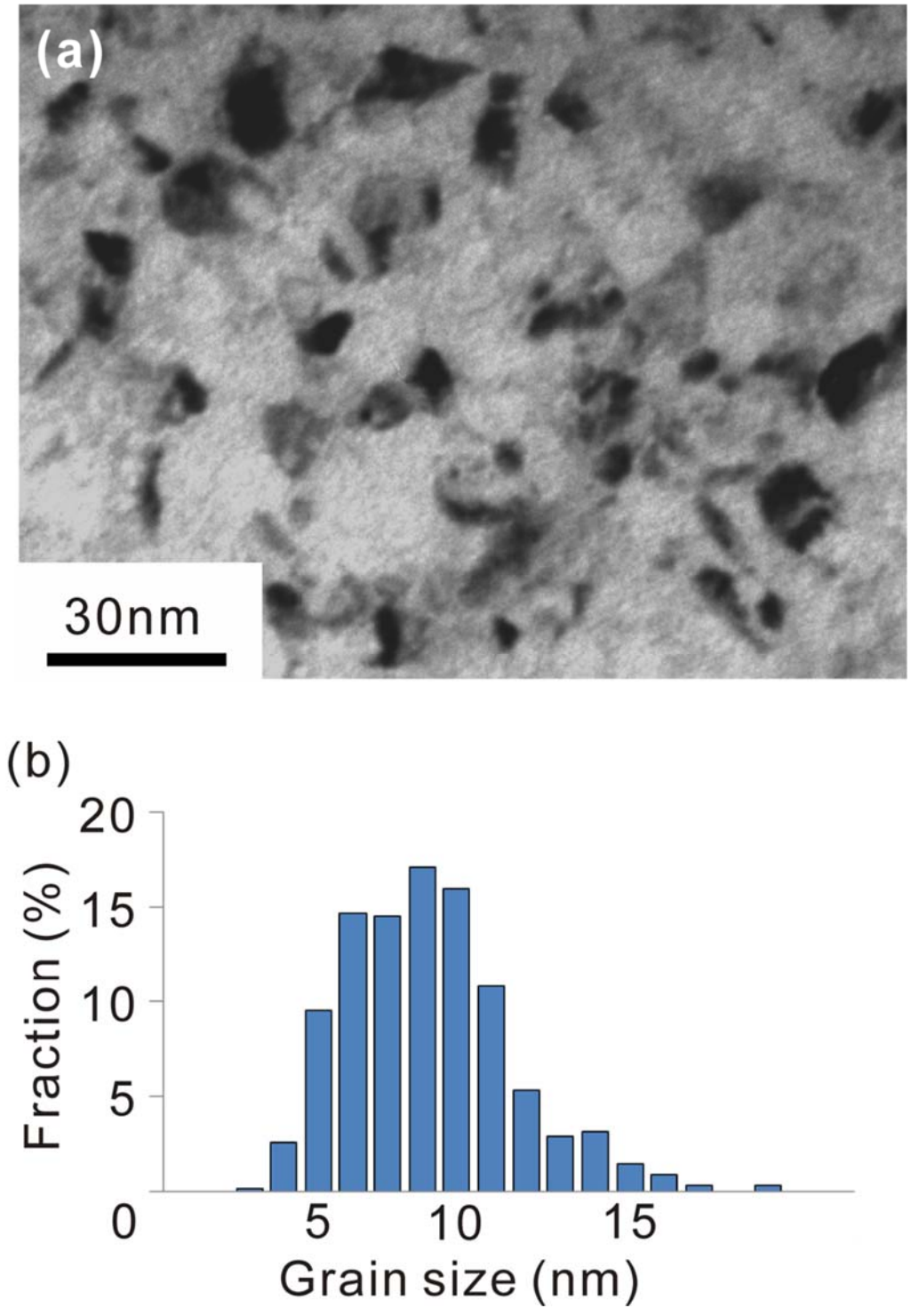

Figure 4-3. (a) Top-view TEM bright field image of ESCE nickel and (b) grain size distribution from more than 500 of grains observed in TEM.

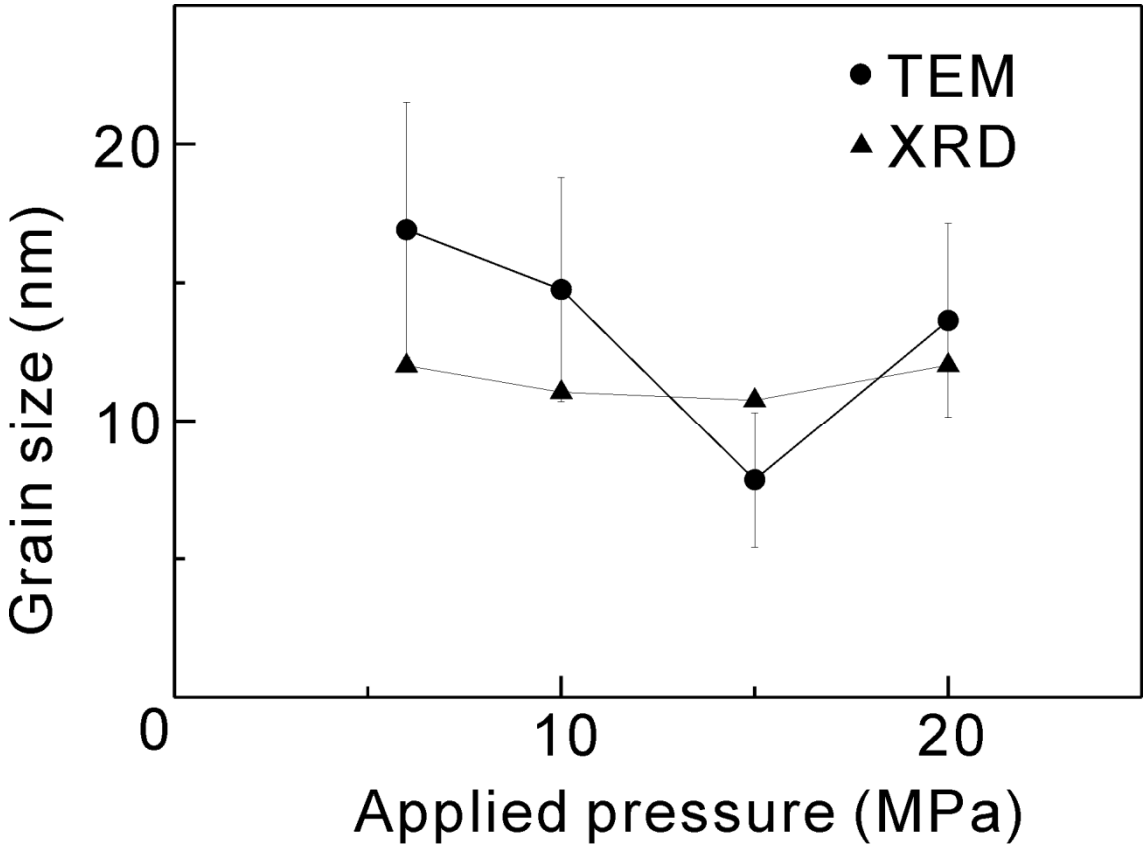

Figure 4-4. Grain size of the films electrodeposited at different pressure evaluated by TEM and XRD

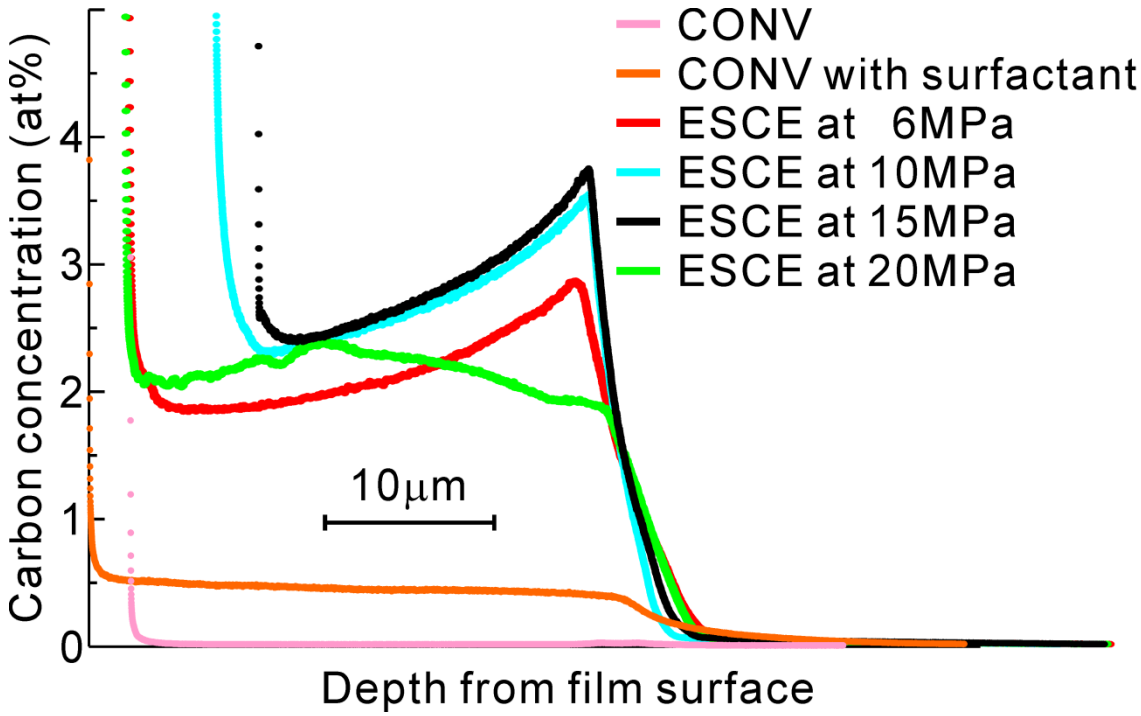

Figure 4-5. Carbon concentration profiles evaluated by GDOES.

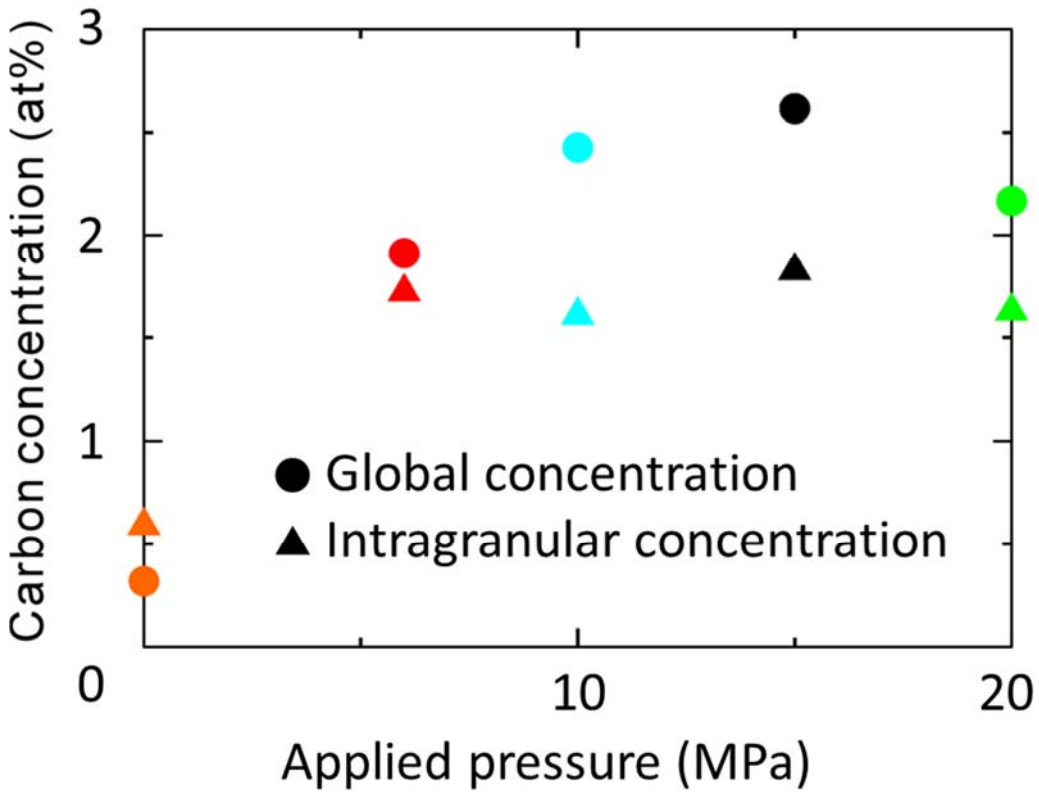

Figure 4-6. Global and intragranular concentrations of carbon in the films plated at different applied pressure. At 0 MPa applied pressure indicates CONV plated film with surfactant, each color corresponded to the samples evaluated in figure 4-5.

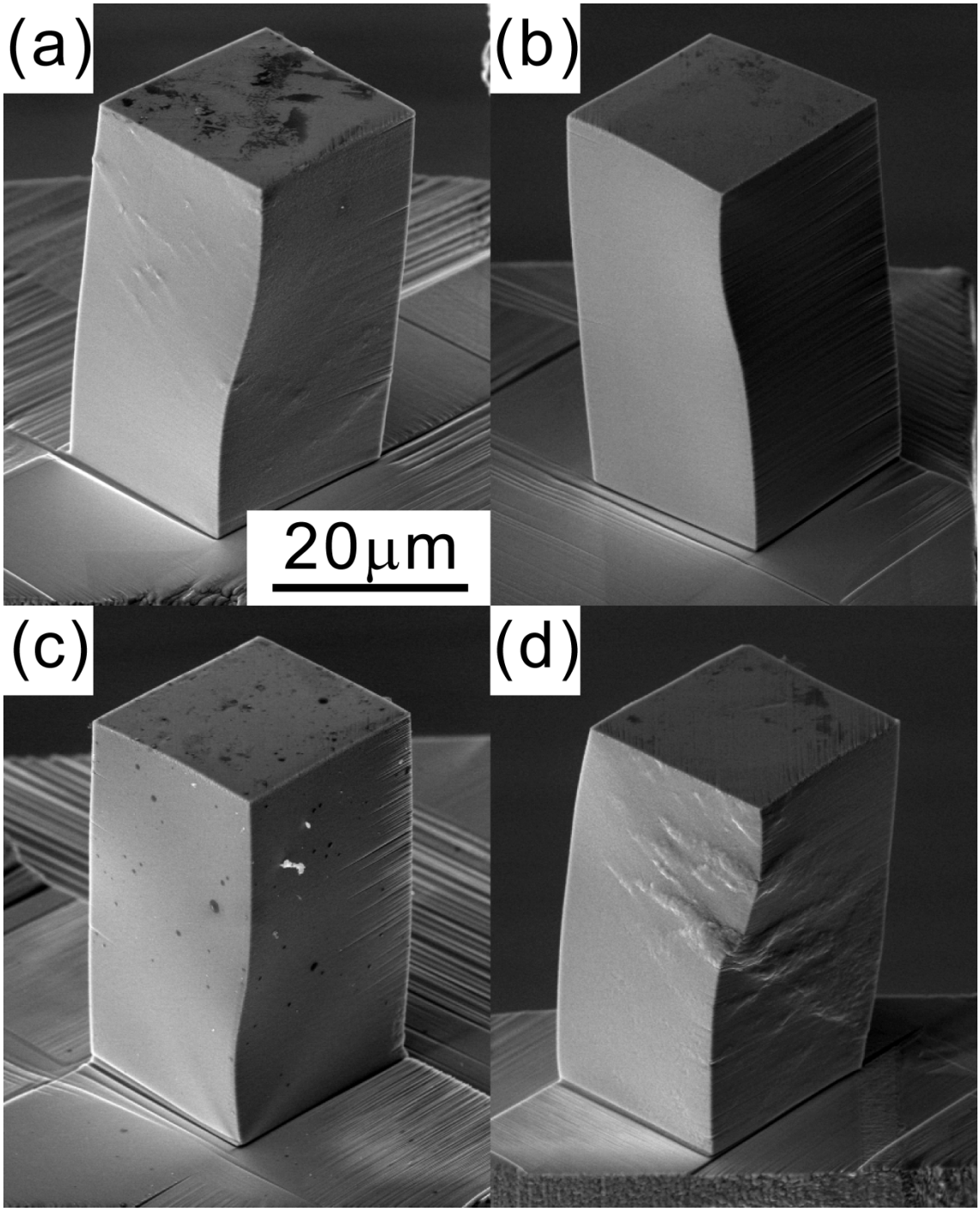

Figure 4-7. SEM images of the deformed pillars (a) 6 MPa, (b) 10 MPa, (c) 15 MPa (d) 20 MPa.

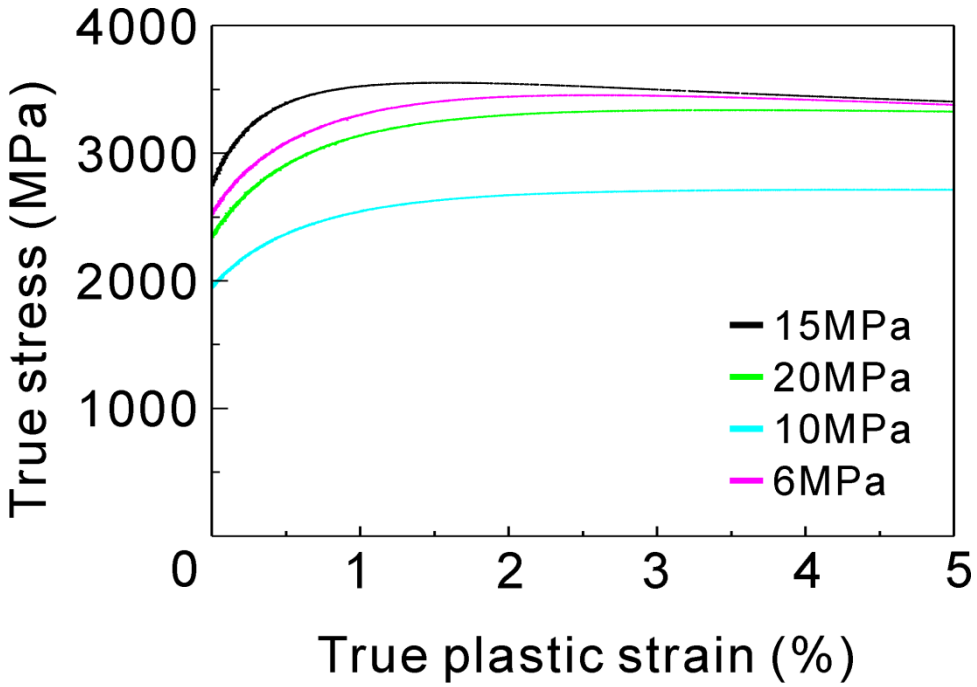

Figure 4-8. True stress-true plastic strain curves of micro-pillar from films electrodeposited at different pressure.

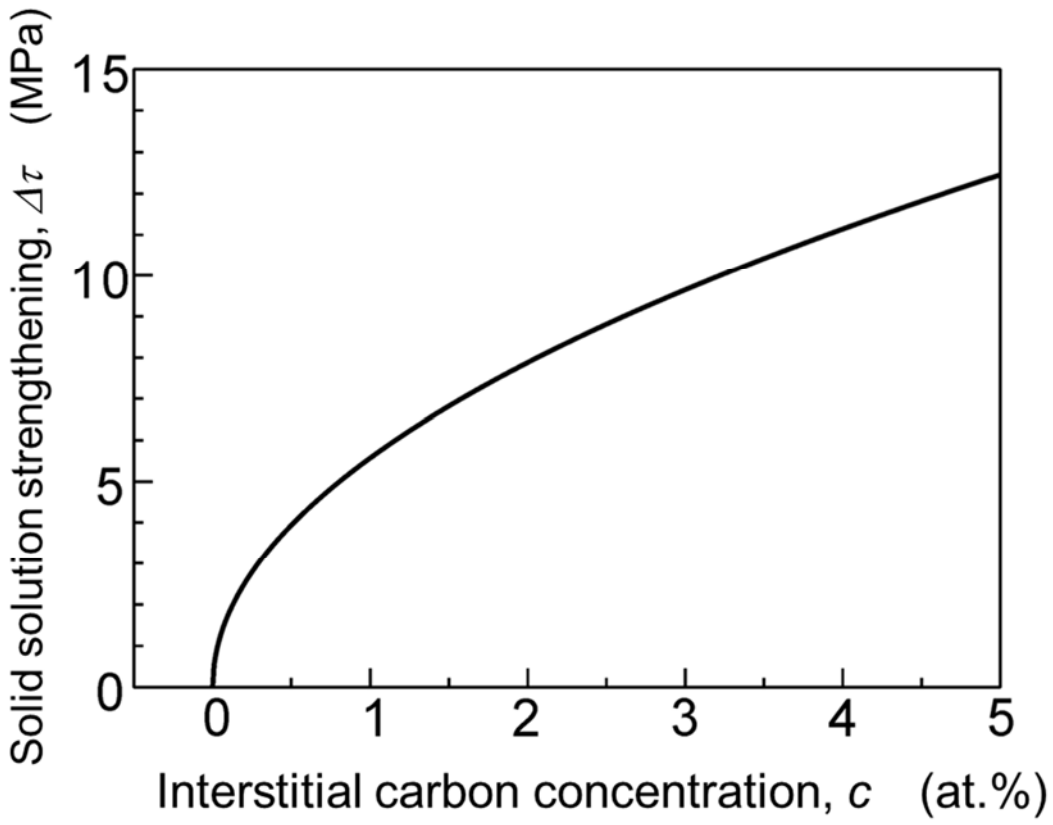

Figure 4-9. The change in solid solution strengthening with interstitial carbon concentration

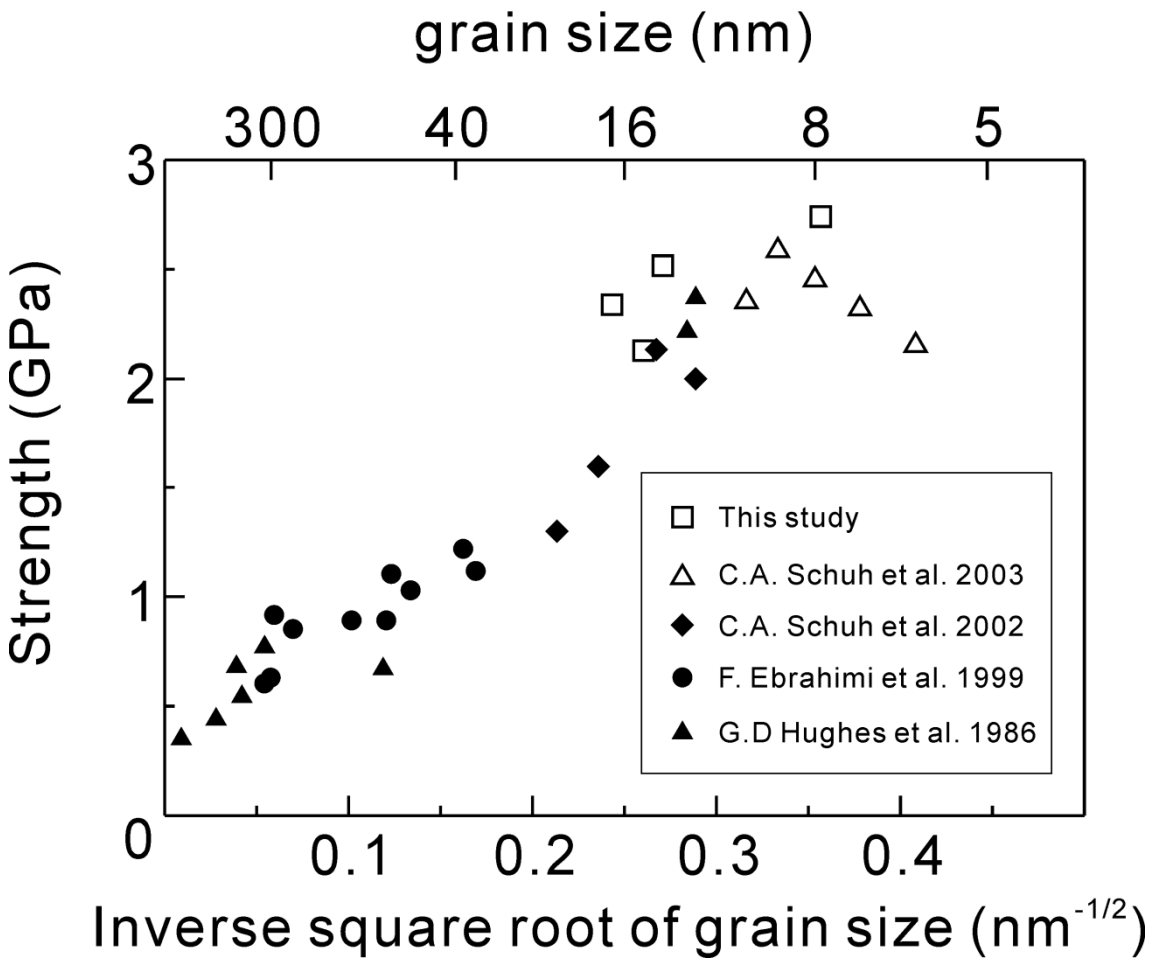

Figure 4-10. H-P plot representing 0.2% yield stress as well as one third of hardness value found in literature.

CHAPTER 5

Sample size effect of electrodeposited nickel with sub-10 nm grain size

5.1 Introduction

The effects of sample size on the mechanical properties have been intensive research topic in decades. Systematical study including experimental and computational approach well agreed to the explanation of size effect, which the strengths is dependent on the size and number of dislocation source for materials deforming via crystallographic slip called dislocation starvation [1]. However, there are only few studies focusing on nanocrystalline materials, especially for materials with grain size less than 10 nm. For deep understanding of sample size effect, investigation of sample size effect on nanocrystalline materials can shed light from different aspect.

Deformations in nanocrystalline metals and alloys often occurs at grain boundary regions i.e., grain boundary mediated deformations, for example, grain

boundary sliding [2] and Coble creep [3] observed. Deformation kinetics is totally different from traditional dislocation mediated deformation, which sample size effect is derived from the dislocation source limited strengthening [1]. Aside from this size effect, two different size effects stated by Armstrong should be considered in polycrystalline materials [4]. One is the well-known H-P effect, and the other is an orientation effect when there are only few grains in cross-section of a specimen. The earlier effect can be eliminated by using materials with the same grain size. However, to avoid the latter effect, ratio between sample size; D and grain size; d, D/d should be maintained large for investigating the extrinsic sample size effect.

In the present work, sample size effects were investigated using non-tapered micro-pillar fabricated from single crystal nickel (SCNi) and electrodeposited nanocrystalline nickel (NCNi) whose grain size is smaller than 10 nm, and sample size is from 5 μm to 30 μm, resulting D/d ratio around 1000.

5.2 Experimental procedures

SCNi was purchased from Nilaco Corporation. NCNi was prepared using an electroplating technique with supercritical CO_2 emulsion [5]. Copper substrates were

pretreated using 10 wt% NaOH solution and 10 wt% HCl solution. Electroplating was conducted with additive-free Watts bath contains 1.0 vol% of polyoxyethylene lauryl ether ($C_{12}H_{25}(OCH_2CH_2)_{15}OH$) for formation of the emulsion. Temperature and pressure were kept constant at 327 K and 15 MPa, respectively. Nanostructured grains were observed by TEM (Philips: CM200).

Different sizes of micro-pillars were fabricated from SCNi and NCNi using FIB (Hitachi: FB-2100) milling at 40 kV with gallium as the liquid metal ion source. To avoid tapering of the pillars due to the redeposition during FIB milling [6], ion irradiation from pillar side was used and square cross-sectional pillar with an aspect ratio of 2:1 were fabricated. Detail of this fabrication method of square pillar was reported in previous work [7], and the method is favorable for fabrication of non-tapered pillar. Zhang et al. studied effect of sample geometry on mechanical test and concluded tapering or misalignment should be avoided [8]. In present work, a shared holder was used in FIB milling and micro-compression testing to minimize misalignment.

Micro-compression tests were conducted with a testing machine equipped with a diamond flat-punch tip, which is assembled in our group and a detailed

description of this testing machine can be found elsewhere [9]. For micro-compression test, displacement rate was controlled for each pillar with different height to allow a strain rate constant of 2.5 X 10^{-3}. Before and after compression, pillars were observed in SEM (Hitachi: S-4500SE) equipped with an EBSD (Oxford instruments: INCA Crystal software).

5.3 Results and discussion

In figure 5-1, plan-view image of electrodeposited NCNi shows uniform and equi-axial grains with an average grain size of 8 nm. The observed uniform and fine grains were caused by a phenomenon named periodic plating characteristic when applying supercritical CO_2 emulsion in electrodeposition [5]. Selected area diffraction pattern shown in the inset of figure 5-1 and the X-ray diffraction analysis (not presented here) showed the electrodeposited nickel was only fcc structure nickel.

SEM images of representative pillars before and after compression were shown in figure 5-2. All the pillars before compression shown in figure 5-2a to d had no tapering owing to the vertical ion irradiation. Prior to the compression,

crystallographic orientation of the SCNi pillars against loading was confirmed by EBSD analysis. Pillar orientation <789> was observed and which is around 5 degrees off from the initial <111> orientation. Multiple slip traces correspond to (111) slip systems were observed in figure 5-2e and 5-2f. NCNi pillars after compression to a strain of approximately 10% showed broad shear crossing from the top front to the bottom (figure 5-2g) and the way crossing (figure 5-2h). This wide shear banding formation has been reported in ultra-fine or nanocrystalline materials [10] during compressive deformation. Such deformation behavior is considered to be because of the extremely low strain hardening capacity while the dislocation storage diminished or deformation mechanism changed to the grain boundary mediated one (grain boundary sliding or Coble creep). From observation of the deformed pillars, similar deformation behavior was observed in each SCNi and NCNi pillars with different sample size, which suggests the deformation mechanism is similar in each case.

Figure 5-3 displays the stress strain curves of pillars with sample size ranging from 5 μm to 30 μm prepared from SCNi and NCNi. Strain was calculated from the displacement measurement of the actuator stage equipped with a diamond indenter. Multiple slip gliding across the pillar or toward the base caused observation

of large work hardening in SCNi pillar compression. This result is similar to the result reported by Frick et al. [11]. Frick et al. reported observation of dislocation lines throughout the pillar and base of the pillar which indicates dislocation interaction between multiple slip and accumulation of dislocation at the pillar base. Thus, the stress needed to activate dislocation source inside the pillar increased with increasing strain. The softening followed is believed to be a result of macroscopic shear by activation of different slip system due to the increased stress. Peak stresses before softening increased with decreasing sample size. For the correlation of the strain amount on micro-compression of NCNi, true plastic strain-true stress curves were illustrated in figure 5-4a with deducting elastic component from the data in figure 5-3b. The NCNi pillar showed extremely high strength, which was 10 times larger than that of SCNi pillar. The high strength was discussed in a previous paper and concluded to be largely because of grain boundary strengthening and enhanced by impurity [7]. The deformation process is believed to be a grain boundary process, such as grain boundary sliding or grain rotation as shown in figure 5-2, which is consistent in all pillars tested. Considering the deformation process, activation of dislocation source, which is believed to be a possible explanation of size dependent strength [1], did not play a role in plastic deformation of nanocrystalline materials.

Thus, the sample size effect on electrodeposited NCNi was not expected. However, micro-compression test shows an obvious increase in both yield stress and flow stress with decreasing sample size from 30 μm to 5 μm.

The stress as a function of pillar diameter for SCNi and NCNi are shown in figure 5-4b. The scaling exponent of -0.25 for peak stress of SCNi is small compared to -0.64 observed by Dimiduk et al. using non-tapered SCNi pillars of <269> oriented [12]. The difference in scaling exponent can be explained by the change in dislocation mechanisms inside the pillars since different loading direction was taken and also the sample size regime is beyond the upper limit of sample size effect as Dimiduk et al. observed as 20 μm [12]. For NCNi, which is expected to deform without dislocation activation, the scaling exponent of -0.125 and -0.057 for 0.2 % offset stress and flow stress at 1 % of plastic strain was observed, respectively. Although the exponent is quite low, yield strength obviously increased from 2.5 GPa to 3.1 GPa when the pillar size decreased from 30 to 5 μm.

On the contrary to the present result, Jang and Greer demonstrated size induced weakening in 60 nm grained nickel nano-pillars with a diameter between 3000 nm and 100 nm [13]. This contradiction can be explained based on the

difference in deformation mechanisms. Jang and Greer observed a transition of deformation mechanisms from dislocation mediated to grain boundary mediated while grain boundary mediated deformation is suggested to be dominated in present work. Rinaldi et al. found increase of strengths with decreasing diameter of pillars from 270 to 160 nm fabricated from NCNi with 30 nm of grain size [14]. Rinaldi et al. conducted statistical analysis on each yield event which can be triggered by activation of a single surface dislocation source, and they proposed a weakest-link theory assuming the number of potential dislocation sources is significantly reduced in small samples. Assumption made by Rinaldi et al. is not applicable in the present case because there are only less than 1 % of grains on the surface of the pillar in this study. Thus the surface effects are negligible.

The size effect in the present NCNi can be considered as a result of grain boundary sliding, which is reported to involve several grains in formation of micro shear band along the grain boundaries. Sums of these shear bands formation will cause macroscopic yield in present micro-compression test. Microscopic strains can generate on the large area of grain boundaries which lies on the same plane with larger shear strain. This corrective motion of grain boundaries has been known as

cooperative grain boundary sliding (CGBS) [15]. Zerin and Mukherjee observed bimodal distribution of sliding offset length on each CGBS event which indicates braking up of large sliding grain block into small grain blocks by secondary CGBS operation. It is observed with increase of strain i.e. work hardening. CGBS events could initiate from flat segment of grain boundaries and the number of these segments decreased when sample size becomes smaller. Larger samples have segments of grain boundaries with longer distance to sliding direction and can deform with smaller stress. This is in good agreement with the change in exponent with increased strain, where large grain blocks in large sample can break up while small samples deform by CGBS with small grain blocks.

5.4 Conclusion

We demonstrated a sample size effect on SCNi and electrodeposited NCNi with grain size of 8 nm. In which, plastic deformation is suggested to be controlled by grain boundary mediated process. Although the scaling exponent of -0.125 for yield stress is very different from that of SCNi, which was -0.25, but the strength increased from 2.5 to 3.1 GPa when the pillar size was decreased from 30 to 5 μm.

Considering CGBS initiated at flat segment of grain boundaries, decrease in the number of these segments with decreasing sample size could be responsible for the sample size effect on NCNi.

5.5 References

[1] J.R. Greer, W.D. Nix, Acta Mater., 53 (2005) 1821.

[2] H. Van Swygenhoven, P.M. Derlet, Phys. Rev. B, 64 (2001) 224105.

[3] J.R. Weertman, Mater. Sci. Eng. A, 166 (1993) 161.

[4] R.W. Armstrong, J. Mech. Phys. Sol., 9 (1961) 196.

[5] T.F.M. Chang, M. Sone, Surf. Coat. Technol., 205 (2011) 3890.

[6] F.A. Stevie, L.A. Giannuzzi, B.I. Prenitzer, *Introduction to focused ion beams: instrumentation, theory, techniques and practice*, New York, Springer Verlag; 2005.

[7] T. Nagoshi, T.F.M. Chang, S. Tatsuo, M. Sone, Microelec. Eng., 110 (2013) 270.

[8] H. Zhang, B.E. Schuster, Q. Wei, K.T. Ramesh, Scripta mater., 54 (2006) 181.

[9] G.P. Zhang, K. Takashima, Y. Higo, Mater. Sci. Eng. A, 426 (2006) 95.

[10] D. Jia, K.T. Ramesh, E. Ma. Acta Mater., 51 (2003) 3495.

[11] C.P. Frick, B.G. Clark, S. Orso, A.S. Schneider, E. Arzt, Mater. Sci. Eng. A, 489 (2008) 319.

[12] D.M. Dimiduk, M.D. Uchic, T.A. Parthasarathy, Acta Mater., 53 (2005) 4065.

[13] A. Rinaldi, P. Peralta, C. Friesen, K. Sieradzki, Acta Mater., 56 (2008) 511.

[14] J.R. Greer, W. Nix, Phys. Rev. B, 73 (2006) 245410.

[15] M. G. Zelin and A. K. Mukherjee, Acta Metall. Mater., 43 (1995) 2359.

5.6 Figures

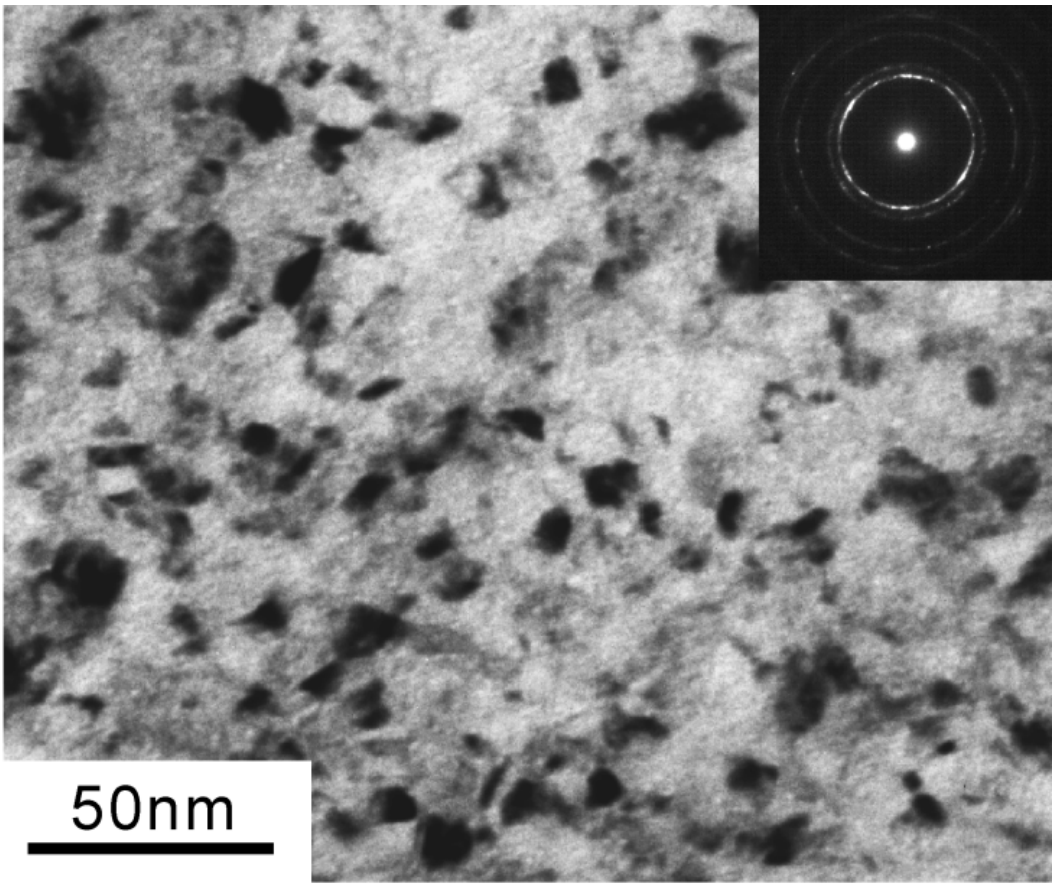

Figure 5-1. Plan-view TEM bright field image of electrodeposited NCNi. Inset shows selected area electron diffraction pattern.

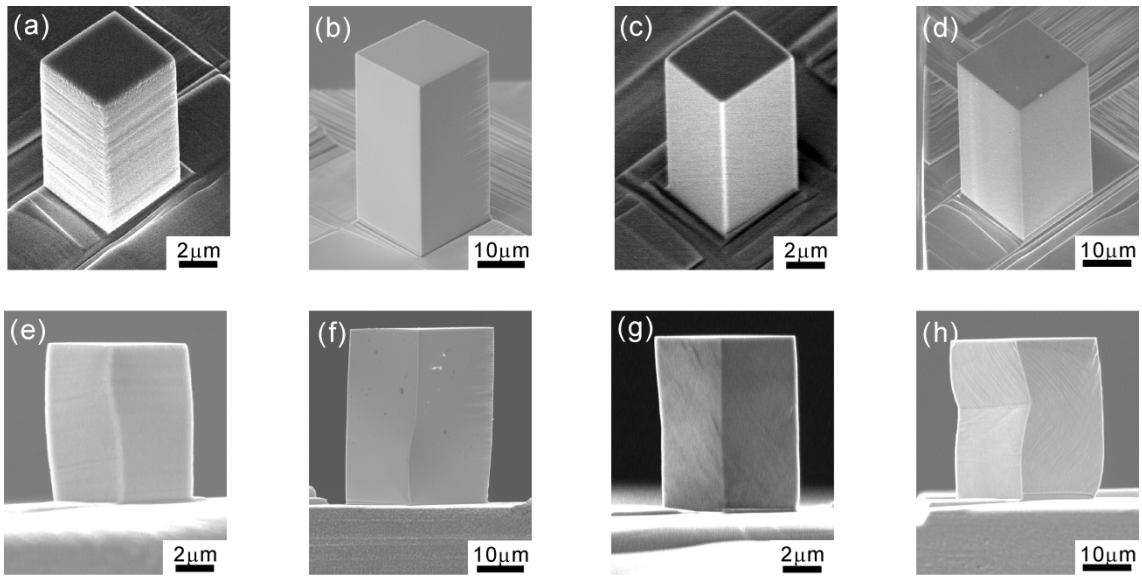

Figure 5-2. SEM images of micro-pillar fabricated from SCNi (a, b) as fabricated, (e, f) deformed and from NCNi (c, d) as fabricated and (g, h) deformed.

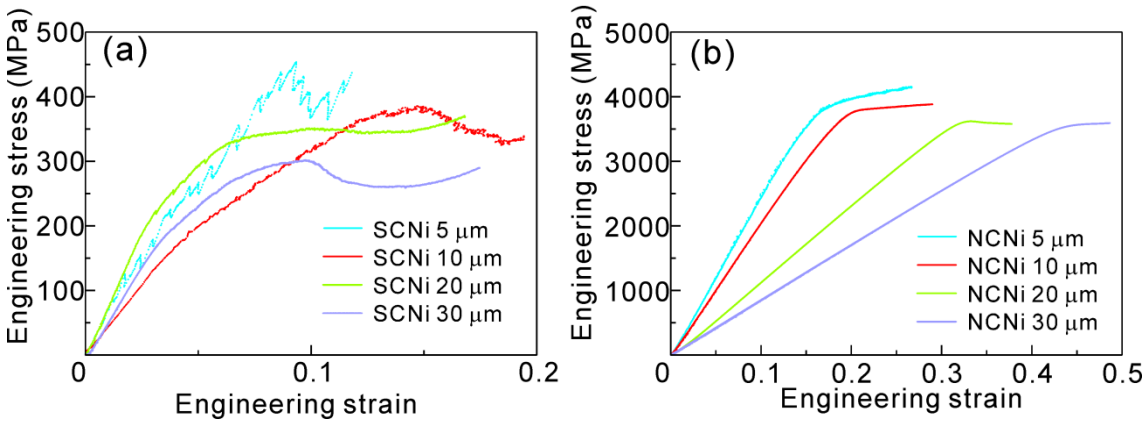

Figure 5-3. Engineering stress-strain curves for micro-compression of (a) SCNi pillars and (b) NCNi pillars with different pillar size.

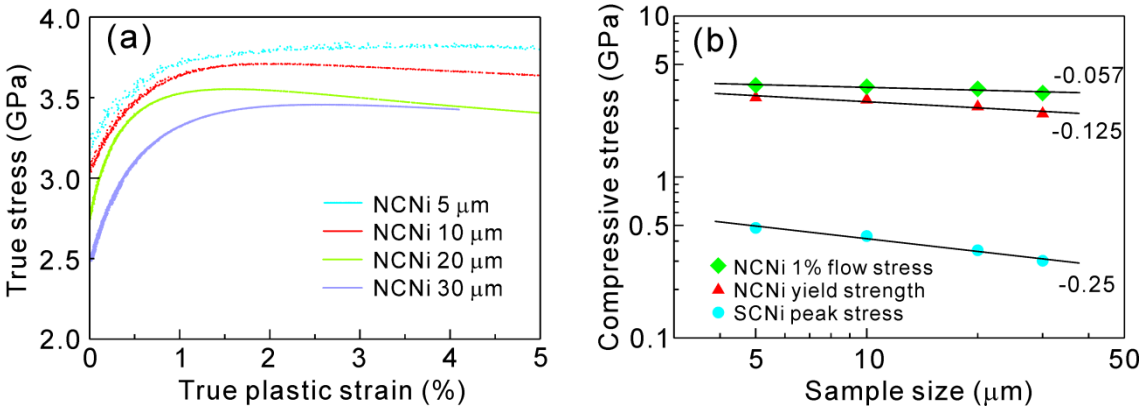

Figure 5-4. (a) True stress-plastic strain curves of NCNi micro-compression delineated from the data obtained in figure 5-3b, and (b) Peak stress for SCNi micro-compression and 1 % flow stress and 0.2 % offset stress for NCNi micro-compression are shown in double-logarithmic graph. Solid lines in (b) are power law fittings and each exponent is shown on the right.

CHAPTER 6

General conclusions

Rectangle pillar for micro-compression testing can be fabricated from any metallic materials at the specific areas of interest. Square pillar fabrication method by FIB milling using vertical irradiations with respect to the pillar loading direction successfully applied for preparation of non-tapered compression pillar. Present work demonstrates the evaluation of mechanical properties of electrodeposited metals with limited dimensions. Mechanical property evaluation using micro-sized specimen can be applied for MEMS and fundamental materials science while evaluations are open for any metals and alloys with thickness of larger than several microns. Conclusions obtained in this work were summarized as follows

Chapter 2

Micro-compression test was conducted on the HPT processed ferrite which possess large strain gradient. While crystal orientation and grain size did not change with increasing strain by HPT process after structural saturation point, grain

boundary misorientation angle distribution became closer to a random distribution which indicates dynamic recrystallization. The micro-compression test reveals site specific mechanical properties of ultrafine grained ferrite. Strength was increased with decreasing grain size and reached to 1.5 GPa accompanied with decrease in elongation. Further increase in HPT strain amount did not change the strength but elongation slightly increased. We suggest these improvements of mechanical properties are because of change of grain boundary structures during dynamic recrystallization.

Chapter 3

Micro-compression test was applied for electrodeposited copper by ESCE and CONV. In contrast to the high carbon content of ESCE nickel, copper film had only slight concentration of carbon. Sub-micron equi-axial grain structure of ESCE copper was changed by 2 months of storage in vacuum at room temperature. Similar microstructures and fractions of twin boundaries suggested self-annealing in both ESCE and CONV plated copper while CONV. Strengths of as-fabricated copper by ESCE was 300 MPa higher than the CONV and , self-annealed ESCE copper, which explained by H-P relationship.

Chapter 4

Mechanical properties of electrodeposited nickel by ESCE at different applied pressure were investigated using micro-compression pillar. Electrodeposited nickel had different grain size around 10 nm with different applied pressure. Highest strength of more than 3.5 GPa was found from nickel with finest grain size of 8 nm which finer than the critical grain size for H-P breakdown reported so far. Suppressed H-P breakdown was explained by the enhanced grain boundary cohesion by impurity carbon which supposed to segregate to the grain boundary.

Chapter 5

Effect of sample size on nanocrystalline nickel with 8 nm grain size was investigated using micro-compression with sample size ranging from 5 μm to 30 μm. Nanocrystalline nickel was found to exhibit size dependent strength with an exponent of -0.056. Although the scaling exponent of -0.125 for yield stress is very different from that of SCNi, which was -0.25, but the strength increased from 2.5 to 3.1 GPa. The decrease in the number of flat segments of grain boundaries for activation of CGBS was suggested to be responsible for the observed sample size effect.

List of Achievements

1st Author Papers:

1. Takashi Nagoshi, Akinobu Shibata, Masato Sone, "Mechanical Behavior on Micro-compression Test in Ultra-low Carbon Steel Produced by High Pressure Torsion", MRS Proceedings, Vol. 1297, p. mrsf10-1297-p10-33, Jan. 2011.
2. Takashi Nagoshi, Tso-Fu Mark Chang, Tatsuo Sato, Masato Sone, "Micro-compression test of nanocrystalline Nickel deposited by supercritical carbon dioxide emulsion", Applied Mechanics and Materials, Vol. 284-287, No. 163, pp. 163-167, Jan. 2013.
3. Takashi Nagoshi, Tso-Fu Mark Chang, Tatsuo Sato, Masato Sone, "Mechanical Properties of Nickel Fabricated by Electroplating with Supercritical CO_2 Emulsion Evaluated by Micro-Compression Test Using Non-Tapered Micro-sized Pillar", Microelectronic Engineering, Vol. 110, pp. 270-273, Sep. 2013.
4. Takashi Nagoshi, Tso-Fu Mark Chang, Tatsuo Sato, Masato Sone, "Sample size effect of electrodeposited nickel with sub-10 nm grain size", Materials Letters, In press.
5. Takashi Nagoshi, Akinobu Shibata, Yoshikazu Todaka, Tatsuo Sato, Masato Sone, "Mechanical behavior of micro-sized pillar fabricated from ultrafine grained ferrite evaluated by micro-compression test", Acta Materialia, Submitted

6. Takashi Nagoshi, Tso-Fu Mark Chang, Tatsuo Sato, Masato Sone, "Suppression of Hall-Petch Breakdown in Nanocrystalline Nickel Electrodeposited Using Supercritical CO_2 Emulsion Evaluated by Micro-Compression Test", Microelectronic Engineering, Submitted

Other Papers:

7. Akinobu Shibata, Takashi Nagoshi, Masato Sone, Shigekazu Morito, Yakichi Higo, "Evaluation of the block boundary and sub-block boundary strengths of ferrous lath martensite using a micro-bending test", Materials Science and Engineering A, Elsevier, Vol. 527, pp. 7538-7544, Oct. 2010.
8. Hirohito Imamura, Takashi Nagoshi, Akari Yoshida, Tso-Fu Mark Chang, Susumu Onaka, Masato Sone, "Evaluation of anisotropic structure in electrodeposited Ni film using micro-sized cantilever", Microelectronic Engineering., Elsevier, Vol. 100, No. C, pp. 25-27, Oct. 2012.
9. Tso-Fu Mark Chang, Takashi Nagoshi, Chiemi Ishiyama, Tatsuo Sato, Masato Sone, "Intact Ultrathin Ni Films Fabricated by Electroplating with Supercritical CO_2 Emulsion", Applied Mechanics and Materials, Vol. 284-287, No. 147, pp. 147-151, Jan. 2013.
10. Eri Shinada, Takashi Nagoshi, Tso-Fu Mark Chang, Masato Sone, "Crystallographic Study on Self-Annealing of Electroplated Copper at Room Temperature," Materials Science in Semiconductor Processing., Elsevier, Vol. 16, pp. 633-639, Apr. 2013.
11. Masahide Mutoh, Takashi Nagoshi, Tso-Fu Mark Chang, Tatsuo Sato,

Masato Sone, “Micro-compression test using non-tapered micro-pillar of electrodeposited Cu”, Microelectronic Engineering, Elsevier, Vol. 111, pp. 118-121, Jun. 2013.

12. Akinobu Shibata, Takashi Nagoshi, Masato Sone, Yakichi Higo., “Micromechanical characterization of deformation behavior in ferrous lath martensite”, Journal of Alloys and Compounds, Elsevier, Vol. 577, No. S1, pp. 555-558, Oct. 2013.

1st Author International Conference (Reviewed):

1. Takashi Nagoshi, Akinobu Shibata, Masato Sone, Yoshikazu Todaka, “Local strength by Micro-compression test in ultra-low carbon steel produced by high pressure torsion” MRS – Fall Meeting 2010, Poster session, Boston (USA) (2010.12)
2. Takashi Nagoshi, Akinobu Shibata, Masato Sone, Yoshikazu Todaka, “The role of grain boundary character distribution on the mechanical behavior of ultra-fine grained ferrite”, E-MRS 2011 FALL MEETING, Oral session, Warsaw (Poland), (2011.9)
3. Takashi Nagoshi, Akinobu Shibata, Masato Sone, Yoshikazu Todaka, “Uniform elongation of ultra-fine grained steels evaluated by micro-compression tests”, International Symposium on Advances in Nanostructured Materials and Applications, The 2011 Acta Materialia Gold Medal Symposium, MS&T 2011 meeting, Poster session, Columbus (USA) (2011.10)

4. Takashi Nagoshi, Tso-Fu Mark Chang, Tatsuo Sato, Masato Sone, “Evaluation of Mechanical properties of electroplated Nickel, 38th International Conference on Micro and Nano Engineering”, 38th International Conference on Micro and Nano Engineering, (MNE2012), Poster session, Toulouse (France) (2012.9)
5. Takashi Nagoshi, Tso-Fu Mark Chang, Tatsuo Sato, Masato Sone, “Micro-compression test of nanocrystalline Nickel deposited by supercritical carbon dioxide emulsion”, ICETI 2012, The 2nd International Conference on Engineering and Technological Innovation, Oral session, Taichung (Taiwan) (2012.11)
6. Takashi Nagoshi, Yuuki Karasawa, Akinobu Shibata, Tatsuo Sato, Masato Sone, “Deformation Behavior of Fully Nano-Twinned BCT Material in a Micro-Compression Test”, MRS - Fall Meeting 2012, Oral session, Boston (USA) (2012.12)
7. Takashi Nagoshi, Masahide Mutoh, Tso-Fu Mark Chang, Tatsuo Sato, Masato Sone, “Sample size effect of electrodeposited nanocrystalline nickel”, Intenational Symposium on Strength of Fine Grained Materials - 60 years of Hall-Petch-, Program & Abstracts of Intenational Symposium on Strength of Fine Grained Materials - 60 years of Hall-Petch-, p. 14, (Japan) (2013.6)
8. Takashi Nagoshi, Tso-Fu Mark Chang, Tatsuo Sato, Masato Sone, “Effect of Pressure on Mechanical Properties of Nickel Film Electrodeposited Using Supercritical CO_2 Emulsion Evaluated by Micro-Compression Test”, MNE2013, 39th International Conference on Micro and Nano Engineering, MNE2013,(UK) (2013.9)

1st Author Domestic Conference:

9. Takashi Nagoshi, Akinobu Shibata, Yoshikazu Todaka, Masato Sone, 160th ISIJ meeting, (Sapporo) (2010.9)
10. Takashi Nagoshi, Akinobu Shibata, Yoshikazu Todaka, Masato Sone, JIM Autumn meeting 2011 (149th), (Okinawa) (2011.11)
11. Takashi Nagoshi, Hikaru Kinashi, Masahide Mutoh, Tso-Fu Mark Chang, Tatsuo Sato, Masato Sone. Japan Institute of Copper annual meeting 2013 (53th), (Osaka) (2013.11)

Other International Conference (Reviewed):

12. Akinobu Shibata, Takashi Nagoshi, Masato Sone, Shigekazu Morito, Yakichi Higo, "Micromechanical characterization of boundary strength in martensitic steel", Materials Science & Technology 2010 (17-21 October, 2010), Materials Science & Technology 2010, Oct. 2010.
13. Hirohito Imamura, Takashi Nagoshi, Akari Yoshida, Tso-Fu Mark Chang, Susumu Onaka, Masato Sone, "Evaluation of anisotropic structure in electrodeposited Ni film using micro-sized cantilever", 37th International Conference on Micro and Nano Engineering, (MNE2011), Elsevier, pp. in press, Sep. 2011.
14. Hirohito Imamura, Takashi Nagoshi, Masato Sone, "Mechanical testing of electrodeposited Ni film parallel and vertical to crystal growth direction using micro-sized cantilever specimens", TACT2011,International Thin Film Conference, TACT2011,International Thin Film Conference, p.

F20110520014, Nov. 2011.

15. Masahide Mutoh, Takashi Nagoshi, Tso-Fu Mark Chang, Masato Sone, “Effect of current density on mechanical properties of electrodeposited Cu film evaluated by micro-pillar compression test method”, ISE2012, 63rd annual meeting of the International Society of Electrochemistry, Aug. 2012.
16. Masahide Mutoh, Takashi Nagoshi, Tso-Fu Mark Chang, Masato Sone, “Micro compression test using non-tapered micro-pillars of electrodeposited Cu”, 38th International Conference on Micro and Nano Engineering, (MNE2012), 38th International Conference on Micro and Nano Engineering, (MNE2012), pp. P202-286, Sep. 2012.
17. Hirohito Imamura, Takashi Nagoshi, Tso-Fu Mark Chang, Tatsuo Sato, Masato Sone, “Multidirectional strength of micro-sized cantilever composed of columnar grains in electrodeposited Ni”, 38th International Conference on Micro and Nano Engineering, (MNE2012), pp. P215-372, Sep. 2012.
18. Tso-Fu Mark Chang, Takashi Nagoshi, Chiemi Ishiyama, Tatsuo Sato, Masato Sone, “Intact Ultrathin Ni Films Fabricated by Electroplating with Supercritical CO_2 Emulsion”, ICETI 2012, The 2nd International Conference on Engineering and Technological Innovation, Nov. 2012.
19. Akinobu Shibata, Takashi Nagoshi, Masato Sone, Shigekazu Morito, Yakichi Higo, “Characterization of local deformation behavior of martensitic steel using a micro-sized cantilever-beam specimen”, 31st Risoe International Symposium on Materials Science (6-10 September 2010), 31st Risoe International Symposium on Materials Science, Sep. 2010.
20. Hirohito Imamura, Takashi Nagoshi, Tso-Fu Mark Chang, Tatsuo Sato,

Masato Sone, “Deformation behavior of electrodeposited Ni film by using micro-compression test”, MRS - Fall Meeting 2012, MRS Proceeding, Dec. 2012.

21. Hikaru Kinashi, Takashi Nagoshi, Tso-Fu Mark Chang, Tatsuo Sato, Masato Sone, “Mechanical Strength of Cu Electroplated in Supercritical CO_2 Emulsion Using Micro-Compression Test”, MNE2013, 39th International Conference on Micro and Nano Engineering, MNE2013, Sep. 2013.
22. Tso-Fu Mark Chang, Takashi Nagoshi, Nao Shinoda, Hikaru Kinashi, Tatsuo Sato, Masato Sone, “Application of Supercritical CO_2 in Electroplating of Ni and Cu”, SuperGreen 2013, The 8th International Conference on Supercritical Fluids, SuperGreen 2013,The 8th International Conference on Supercritical Fluids, Oct. 2013.
23. Hikaru Kinashi, Tetsuya Shimizu, Takashi Nagoshi, Tso-Fu Mark Chang, Tatsuo Sato, Masato Sone, “Glow discharge optical emission spectroscopic study of Cu film fabricated by electrodepostion using supercritical CO_2 emulsified electrolyte”, TACT2013, International Thin Films Conference, TACT2013, Oct. 2013.
24. Masato Sone, Tetsuya Shimizu, Tso-Fu Mark Chang, Yuma Ishimoto, Hikaru Kinashi, Takashi Nagoshi, Tatsuo Sato, “Nanoscale Wiring By Cu Electrodeposition in Supercritical Carbon Dioxide”, 224th ECS Meeting, ECS, Nov. 2013.

Acknowledgements

First of all, I would like to appreciate my supervisor, Associate Professor Masato Sone, for his constant encouragement and advice. It would not have been possible to finish my Doctor thesis without his support. I would like to extend my sincere appreciation to Emeritus Professor Yakichi Higo, Professor Tatsuo Sato, Professor Hideki Hosoda, and Associate Professor Tomonari Inamura for their valuable guidance and suggestion. Deepest gratitude is also given to Professor Masaharu Kato, Professor Susumu Onaka, Professor Fumihiro Wakai and Professor Shinji Kumai for their critical comments and suggestions.

Thanks also to all the past and present members of our group, Assistant Professor Tso-Fu Mark Chang, Mr. T. Tasaki, Ms. E. Shinada, Mr. N. Yoshida, Mr. Y. Karasawa, Mr. T. Uemura, Mr. H. Imamura, Mr. M. Mutoh, Ms N. Shinoda, Mr. H. Nagai, Mr. Y. Ishimoto, Mr. H. Kinashi, Mr. T. Aoki, Mr. T. Oda, Mr. Y. Kihara, Ms. M. Tanabe and Mr. B. Zheng. Especially Prof. Mark had given me much advice and support. I would like to express thank to Assistant Professor Akinobu Shibata, Ms. Chiemi Ishiyama for their precious instruction and suggestion. I also appreciate to the member of Hosoda and Inamura group for their help.

Last I would like to thank my family for their countless support and understanding.

Takashi Nagoshi